

Redox-switchable carboranes for uranium capture and release

<https://doi.org/10.1038/s41586-019-1926-4>

Received: 26 March 2019

Accepted: 30 October 2019

Published online: 22 January 2020

Megan Keener¹, Camden Hunt¹, Timothy G. Carroll¹, Vladimir Kampel², Roman Dobrovetsky², Trevor W. Hayton¹ & Gabriel Ménard^{1*}

The uranyl ion (UO_2^{2+} ; U(VI) oxidation state) is the most common form of uranium found in terrestrial and aquatic environments and is a central component in nuclear fuel processing and waste remediation efforts. Uranyl capture from either seawater or nuclear waste has been well studied and typically relies on extremely strong chelating/binding affinities to UO_2^{2+} using chelating polymers^{1,2}, porous inorganic^{3–5} or carbon-based^{6,7} materials, as well as homogeneous⁸ compounds. By contrast, the controlled release of uranyl after capture is less established and can be difficult, expensive or destructive to the initial material^{2,9}. Here we show how harnessing the redox-switchable chelating and donating properties of an *ortho*-substituted *closo*-carborane (1,2-(Ph_2PO)₂-1,2- $\text{C}_2\text{B}_{10}\text{H}_{10}$) cluster molecule can lead to the controlled chemical or electrochemical capture and release of UO_2^{2+} in monophasic (organic) or biphasic (organic/aqueous) model solvent systems. This is achieved by taking advantage of the increase in the ligand bite angle when the *closo*-carborane is reduced to the *nido*-carborane, resulting in C–C bond rupture and cage opening. The use of electrochemical methods for uranyl capture and release may complement existing sorbent and processing systems.

Known for over 50 years, carboranes have been extensively studied in coordination chemistry (including with U), catalysis, luminescence, and energy storage applications^{10–15}. Studies have shown that reduction of substituted *closo*-carboranes to the *nido*-carboranes results in rupture of the C–C bond and cage opening, with a simultaneous increase in ligand bite angle, θ (Fig. 1a; *closo* and *nido* refer to $2n + 2$ and $2n + 4$ framework bonding electrons, respectively, where n is the number of vertices)^{11,14,16–18}. We rationalized that by incorporating donating groups to *ortho*-carborane, we could tune the chelating properties of the cluster switching from opened to closed conformations by redox control of the reduced and oxidized states, respectively, and enable the chemical or electrochemical capture and release of uranyl in solution (Fig. 1a).

The *closo*-carborane 1,2-(Ph_2PO)₂-1,2- $\text{C}_2\text{B}_{10}\text{H}_{10}$ (**1**) was synthesized and fully characterized, including by X-ray diffraction (XRD) studies (Fig. 1a, Extended Data Fig. 1a)¹⁹. The cage C–C bond length (1.688(4) Å) and interatomic P...P distance (3.537 Å) are consistent with previous relevant reports^{19,20} (all uncertainties are estimated standard deviations or standard uncertainties). These metrics will be used throughout to correlate coordinated and uncoordinated carboranes, both in lieu of—yet proportional to—the traditional bite angle θ (Fig. 1a). The cyclic voltammogram of **1** in tetrahydrofuran (THF) revealed two quasi-reversible cathodic waves at –0.93 V and –1.11 V relative to the ferrocene/ferrocenium (Fc/Fc⁺) redox couple (Extended Data Fig. 2a). Reduction of **1** using 2.0 equiv. decamethylcobaltocene (CoCp₂) afforded the direduced *nido*-carborane, [CoCp₂]₂[(*nido*-1,2-(Ph_2PO)₂-1,2- $\text{C}_2\text{B}_{10}\text{H}_{10}$)] (**2a**) (Fig. 1a). The solid-state structure revealed an open-cage *nido*-carborane with a

cleaved C–C bond (2.860 Å) and an elongated P...P distance (5.036 Å) relative to **1** (Extended Data Figs. 1b, c). An analogous salt, [Bu₄N]₂[(*nido*-1,2-(Ph_2PO)₂-1,2- $\text{C}_2\text{B}_{10}\text{H}_{10}$)] (**2b**) (Fig. 1a), relevant to the electrochemical experiments, was also synthesized by reduction of **1** with K₂C₈, followed by salt metathesis with [Bu₄N][Cl] (see Methods).

We next investigated the coordination chemistry of **1** and **2a**. Addition of 4 equiv. **1** to dimeric [UO₂Cl₂(THF)₂]₂ in deuterated dichloromethane (DCM-d₂) resulted in a light-yellow solution from which two new equivalent-intensity ³¹P resonances appeared at 38.8 and 38.4 ppm in the nuclear magnetic resonance (NMR) spectrum, shifted downfield from **1** (22.8 ppm). The inequivalent P environments suggest either an octahedral geometry at U with two monodentate **1** ligands or a pentagonal bipyramidal geometry at U with two bidentate **1** and a chloride in the fifth equatorial site. Although attempts to obtain single crystals for XRD studies failed, the NMR data suggest that a 2:1 adduct is formed with a presumed formulation of UO₂Cl₂(**1**)₂. In contrast to **1**, treatment of 2 equiv. **2a** to [UO₂Cl₂(THF)₂]₂ led to clean formation of a single new resonance at 51.1 ppm in the ³¹P NMR spectrum, consistent with a bidentate coordination mode. XRD studies confirmed the composition as the uranyl salt [CoCp₂]₂[UO₂Cl₂(*nido*-1,2-(Ph_2PO)₂-1,2- $\text{C}_2\text{B}_{10}\text{H}_{10}$)] (**3**) (Fig. 1a, c). A disubstituted uranyl salt was also obtained by addition of 4 equiv. **2a** to [UO₂Cl₂(THF)₂]₂. Monitoring the reaction by ³¹P NMR spectroscopy revealed clean conversion to a new product with a single peak at 52.0 ppm. XRD studies on single crystals confirmed the composition as the disubstituted complex [CoCp₂]₂[UO₂(*nido*-1,2-(Ph_2PO)₂-1,2- $\text{C}_2\text{B}_{10}\text{H}_{10}$)₂] (**4**) (Fig. 1a, b). The bond metrics for **3** and **4** are similar (Extended Data Fig. 1c).

¹Department of Chemistry and Biochemistry, University of California, Santa Barbara, CA, USA. ²School of Chemistry, Raymond and Beverly Sackler Faculty of Exact Sciences, Tel Aviv University, Tel Aviv, Israel. *e-mail: menard@chem.ucsb.edu

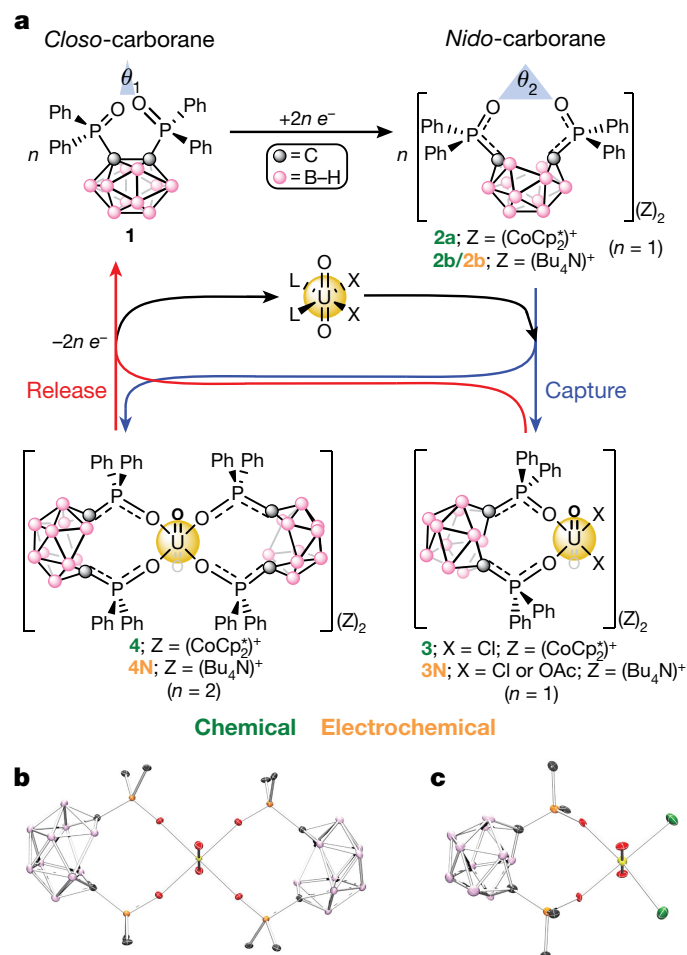


Fig. 1 | Chemical or electrochemical capture and release of UO_2^{2+} with resulting complexes shown. **a**, General chemical or electrochemical mono- or bi-phasic capture of uranyl from $UO_2X_2L_2$ ($X = Cl^-, OAc^-$; $L = THF, Ph_3PO$) using the reduced ‘open’-cage *nido*-carboranes (**2a/2b**) generated by reduction (for example, $CoCp_2$ or negative bias) of the ‘closed’-cage *closo*-carborane (**1**). The corresponding relative bite angles (θ) are also shown. Oxidation (for example, $[FeCp_2][PF_6]$ or positive bias) of the captured products **3/4** or **3N/4N** leads to UO_2^{2+} release. Compounds labelled in green have been chemically isolated, whereas compounds in orange are proposed electrochemical products (see Methods). Blue and red pathways represent UO_2^{2+} capture and release, respectively. **b, c**, Solid-state molecular structures of **4** (**b**) and **3** (**c**) obtained from XRD studies. H atoms, $[CoCp_2]^+$ counter cations, phenyl C–H linkages and all co-crystallized solvent molecules are omitted for clarity. See Extended Data Fig. 1 for the structures of **1** and **2a**.

Whereas **1** and **2a** coordinate to UO_2^{2+} , we postulated that a third ligand with a competitive binding affinity to **1**, but weaker than **2a**, could enable a pathway to UO_2^{2+} release. Competition experiments using **1**, **2a** and triphenylphosphine oxide (TPO), as part of $UO_2Cl_2(TPO)_2$ (ref. 21), were performed and monitored by $^{31}P\{^1H\}$ NMR spectroscopy in $DCM-d_2$. Two equivalents of **1** were added to $UO_2Cl_2(TPO)_2$ for a 1:1 molar ratio of **1**:TPO. After an equilibration period, the $^{31}P\{^1H\}$ NMR spectrum revealed broadened resonances for $UO_2Cl_2(TPO)_2$ and free TPO, as well as a set of sharp resonances for $UO_2Cl_2(\mathbf{1})_2$ and free **1**. The ratio of $UO_2Cl_2(\mathbf{1})_2$:**1** was determined to be approximately 1:3, suggesting an equilibrium favouring the adduct, $UO_2Cl_2(TPO)_2$ (Extended Data Fig. 3a). The binding affinity of TPO was next compared to **2a** by addition of 1 equiv. **2a** to $UO_2Cl_2(TPO)_2$. Rapid precipitation of products was observed. The $^{31}P\{^1H\}$ NMR spectrum of the DCM supernatant revealed complete conversion to the products **3** and **4**, along with a sharp singlet for TPO, and a minor unknown singlet at 47 ppm. Analysis of the precipitate dissolved

in propylene carbonate (PC) by $^{31}P\{^1H\}$ NMR spectroscopy revealed the presence of **4** (Extended Data Fig. 3b). These data are consistent with full dissociation of TPO from $UO_2Cl_2(TPO)_2$ in the presence of **2a**. The binding affinity of TPO was next tested against PC, a coordinating solvent²². An initial $^{31}P\{^1H\}$ NMR spectrum of $UO_2Cl_2(TPO)_2$ dissolved in $DCM-d_2$ revealed two singlets in a 3:1 ratio at 48.09 and 47.97 ppm, respectively, probably arising from *trans:cis* isomerism²³. Whereas addition of 2 equiv. PC led to negligible changes, addition of 20 and 40 equivalents led to increasing broadness of the aromatic peaks in the 1H NMR spectra and broadening of the singlets in the $^{31}P\{^1H\}$ NMR spectra (Extended Data Fig. 4). Together, these data suggest a weak equilibrium with PC that is heavily shifted towards $UO_2Cl_2(TPO)_2$. Density functional theory (DFT) calculations further supported these observations. The electron density surfaces with integrated electrostatic potentials for **1** and **2a** clearly indicate increased electron density at the P = O bonds of **2a** upon reduction, accounting for its experimentally observed increased Lewis basicity (Extended Data Fig. 1d). This probably complements the increased bite angle (Fig. 1a) in rendering **2a** a stronger chelating agent than **1**. In silico isodesmic reactions of **2a**/TPO, TPO/**1** or **1**/PC with protons as a model for the uranyl cation were also calculated (see Methods and Supplementary Information). Together with the experimental data, these data support a relative Lewis basicity trend of: **2a** \gg TPO $>$ **1** \gg PC.

We next investigated the in situ chemical capture and release of UO_2^{2+} . For optimal solubility, we used a 3:1 PC:benzene solvent mixture. A 2:4 solution of **1**:TPO was analysed by $^{31}P\{^1H\}$ NMR spectroscopy, which revealed two sharp resonances (Extended Data Fig. 5a). Addition of 0.5 equiv. $[UO_2Cl_2(THF)_2]$ (1 equiv. U) resulted in no appreciable change to the resonance for **1**, but in substantial broadening to the resonance for TPO (Extended Data Fig. 5b). Only trace $UO_2Cl_2(TPO)_2$ is observed and is probably due to a combination of rapid exchange with excess TPO and the excess ($\sim 2,000$ times) PC used relative to U. To initiate chemical capture of UO_2^{2+} , 4 equiv. $CoCp_2$ was added. Analysis by $^{31}P\{^1H\}$ NMR spectroscopy revealed the rapid and complete conversion of **1** to **4** with concomitant release of TPO (Extended Data Fig. 5c). To initiate UO_2^{2+} release, we first determined the oxidation potential of **4** by cyclic voltammetry, which revealed a quasi-reversible anodic event at -0.42 V relative to Fc/Fc^+ (Extended Data Fig. 2b). Thus, we exposed our in situ generated solution of **4** and TPO to 4 equiv. $[Fc][PF_6]$. Analysis by $^{31}P\{^1H\}$ NMR spectroscopy revealed the full conversion of **4** back to **1**, along with the re-appearance of a broadened TPO resonance, similar to that of the pre-reduced solution (Extended Data Fig. 5d). Together, these results demonstrate the successful chemical capture and release of UO_2^{2+} in solution.

We next targeted the electrochemical capture and release of UO_2^{2+} by galvanostatic bulk electrolysis (GBE). This was conducted using a divided H-cell with coiled Pt electrodes, an anion-exchange membrane (AEM) and an excess of the Fc/Fc^+ redox couple in the counter compartment (Fig. 2a). A 0.5:5:6 ratio of $[UO_2Cl_2(THF)_2]_2$:**1**:TPO was used in PC:benzene (3:1) along with an internal standard for ^{31}P NMR integration. Whereas the use of excess TPO is well reasoned (see above), the use of excess **1** was found to be necessary for optimal electrochemical performance (see Methods). An initial $^{31}P\{^1H\}$ NMR spectrum revealed a sharp signal for **1** and a broadened signal for TPO (Fig. 2b, initial), analogous to the chemical capture/release experiments. Electrochemical capture of UO_2^{2+} was initiated by galvanostatically charging the solution to a 75% theoretical state of charge (SOC) relative to the UO_2^{2+} concentration (Fig. 2c, blue; see Methods). Analysis of the reaction mixture by $^{31}P\{^1H\}$ NMR spectroscopy revealed the conversion of **1** to the captured products **3N** ($X = Cl$) and **4N**—the analogues of **3** and **4**, but with $[Bu_4N]^+$ cations (Fig. 1a)—with release of all TPO, as determined by integration versus the internal standard (Fig. 2b, cycle 1, blue; Extended Data Fig. 6a). To initiate the electrochemical release of UO_2^{2+} , the cell was galvanostatically discharged to a final SOC of 15% (Fig. 2c, red; the SOC extrema of 0% and 100% were not used, to avoid unwanted

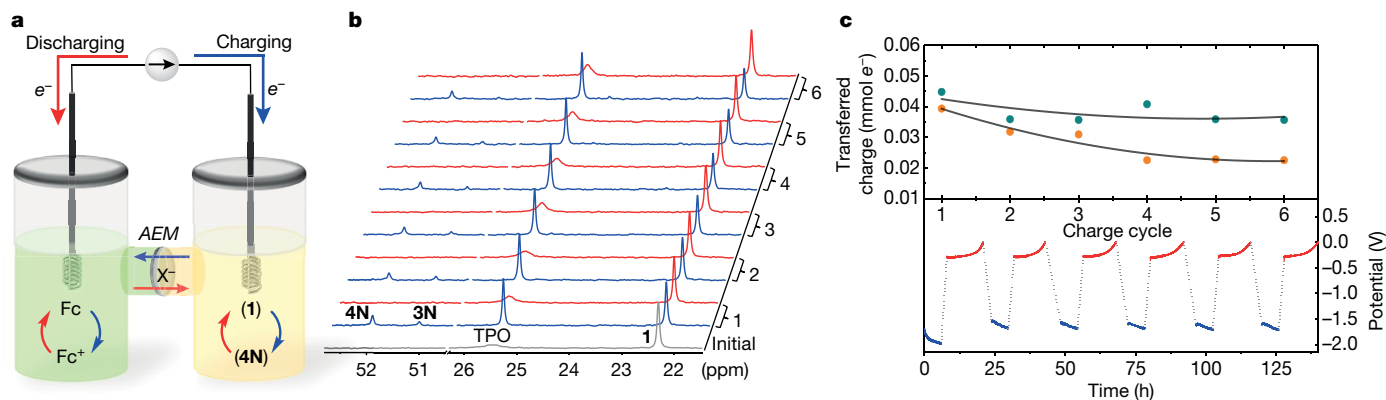


Fig. 2 | Electrochemical setup and quantification data for the capture (blue) and release (red) of UO_2^{2+} in solution. a, Illustration of the H-cell used, incorporating excess Fc/Fc^+ (left) and **1**, TPO and $[\text{UO}_2\text{Cl}_2(\text{THF})_2]$ (right) in a 3:1 PC:benzene solvent mixture. Charging the cell (blue) leads to the capture of UO_2^{2+} , converting **1** to **4N** (major product) and **3N** (minor product, not shown). **b**, Quantification of products and reactants by $^{31}\text{P}\{^1\text{H}\}$ NMR spectroscopy against an inert internal standard, $[\text{Ph}_3\text{PNPPPh}_3][\text{PF}_6]$ (not shown). The initial spectrum is shown in grey, whereas spectra acquired during charge and

discharge cycles (1–6) are shown in blue and red, respectively. **c**, Bottom, applied galvanostatic potentials for charge (blue) and discharge (red) cycles. Dashed lines represent wait periods, which were necessary for $^{31}\text{P}\{^1\text{H}\}$ NMR data acquisition. Each cycle is 24 h. Top, instrumental measure of delivered charge (teal) versus charge used for the reduction of **1**, measured by quantifying the total reduced products, **3N** and **4N**, by ^{31}P NMR spectroscopy. See Methods and Extended Data Figs. 6, 8 for additional experimental details and data.

secondary electrochemical processes²⁴). Analysis of the reaction mixture by $^{31}\text{P}\{^1\text{H}\}$ NMR spectroscopy revealed the full conversion of **3N** and **4N** back to **1**, along with the presence of a broadened TPO resonance (Fig. 2b, cycle 1, red). The capture and release by GBE was carried out over the course of another five full cycles (Fig. 2c), with analyses of the reaction mixtures by $^{31}\text{P}\{^1\text{H}\}$ NMR spectroscopy after each run (Fig. 2b). We observed that repeated cycling resulted in a loss of electrochemically generated **3N**, which we attribute to chloride migration to the counter compartment over time. The gradual appearance of a minor unknown product with a ^{31}P resonance at 45 ppm was also observed after each charge cycle (Extended Data Fig. 6a). Analysis of the $^{31}\text{P}\{^1\text{H}\}$ NMR integrations revealed approximate average losses of 0.3% per cycle for TPO, 3.4% per cycle for **4N** and 7.2% per cycle for **1**, perhaps attributable to electrochemical side reactions (Extended Data Fig. 6b)^{25,26}. Lastly, analysis of the measured instrumental charge transferred relative to the total charge transferred for UO_2^{2+} capture (determined by $^{31}\text{P}\{^1\text{H}\}$ NMR integrations) revealed a plateauing trend with increasing cycle number, with differences in charge attributed to Faradaic losses (Fig. 2c, top). Together, these results demonstrate the successful monophasic electrochemical capture and release of UO_2^{2+} .

A biphasic extraction scheme involving dissolved UO_2^{2+} (from $\text{UO}_2(\text{NO}_3)_2(\text{THF})_2$) in the aqueous phase and **1** in the organic phase was next explored as a model system (Fig. 3a)²⁷. We switched solvents from PC to water-immiscible 1,2-dichloroethane (DCE) and modified our H-cell design to include a physical glass-frit separator coupled with a heterogeneous carbon additive acting as a capacitive buffer, analogous to a previous report²⁸, owing to the incompatibility of DCE with the anion-exchange membrane. The capture and release of UO_2^{2+} was simultaneously monitored by $^{31}\text{P}\{^1\text{H}\}$ NMR and ultraviolet–visible absorption (UV-Vis) spectroscopy for the organic and aqueous layer, respectively. We note that the vibronic ligand-to-metal charge transfer absorption of UO_2^{2+} (425 nm) is pH-dependent, resulting in a variable extinction coefficient (ϵ)^{29,30}; therefore, a buffered solution of UO_2^{2+} was used. Figure 3 outlines the simplified experimental setup displaying half of the H-cell (see Methods and Extended Data Figs. 7, 8 for the full cell design and methodology). A DCE solution of **1** (1.0 equiv.) with $[\text{Bu}_4\text{N}][\text{PF}_6]$ as the supporting electrolyte was galvanostatically charged to a ~75% theoretical SOC. Analysis of the solution by $^{31}\text{P}\{^1\text{H}\}$ NMR spectroscopy revealed the clean conversion of most of **1** to **2b** (Fig. 3a, Extended Data Fig. 9a). A sodium acetate (NaOAc)-buffered (pH 5.4) water solution containing 1.25 equiv. $\text{UO}_2(\text{NO}_3)_2(\text{THF})_2$ was

next added to the DCE layer with mixing. Approximately 0.9 equiv. UO_2^{2+} was captured from the aqueous phase, as evidenced by the comparison of the UV-Vis spectra obtained before and after mixing with the charged DCE solution (Fig. 3a, b, Extended Data Fig. 10a). Analysis of the DCE solution by $^{31}\text{P}\{^1\text{H}\}$ NMR spectroscopy revealed the clean formation of a single resonance at 51.5 ppm (Fig. 3b, Extended Data Fig. 9b). Given the similar chemical shifts of isolated complexes **3** (51.1 ppm) and **4** (52.0 ppm), as well as the quantity of UO_2^{2+} captured (0.9 equiv.), we propose that the uranyl is probably the mono-ligated **3N** ($\text{X} = \text{OAc}^-$ because of the buffer); however, **4N** cannot definitively be excluded (Fig. 1a). The aqueous phase was next removed and the cell was galvanostatically discharged to achieve a theoretical final SOC of ~0%. Mixing a fresh NaOAc -buffered solution (pH 5.4) into this solution led to the release of approximately 0.5 equiv. UO_2^{2+} from the DCE layer, as confirmed by UV-Vis spectroscopy (Fig. 3c, Extended Data Fig. 10b). Analysis of the DCE layer by $^{31}\text{P}\{^1\text{H}\}$ NMR spectroscopy revealed the near-quantitative conversion to **1**, as well as the formation of minor (~20%) unknown byproducts (Fig. 3c, Extended Data Fig. 9c). We propose that the acetate ions probably act as the biphasic analogue of the monophasic TPO ligands by competitively binding with **1** to UO_2^{2+} . Control experiments revealed that negligible biphasic capture of UO_2^{2+} from the NaOAc -buffered solution occurred in the presence or absence of **1** (see Methods and Extended Data Fig. 10c–f). Together, these biphasic GBE experiments demonstrate the potential applicability of this redox-switchable capture and release chemistry.

In summary, we have introduced an approach to uranyl management involving its capture and—importantly—its release by controlled redox-switchable chelation using a derivatized *ortho*-carborane in monophasic or biphasic (organic/aqueous) environments. We anticipate that this fundamentally new direction in cluster carborane chemistry will have a considerable impact on nuclear fuel extraction and waste sequestration activities, and may lead to new research directions in related metal capture and release activities.

Online content

Any methods, additional references, Nature Research reporting summaries, source data, extended data, supplementary information, acknowledgements, peer review information; details of author contributions and competing interests; and statements of data and code availability are available at <https://doi.org/10.1038/s41586-019-1926-4>.

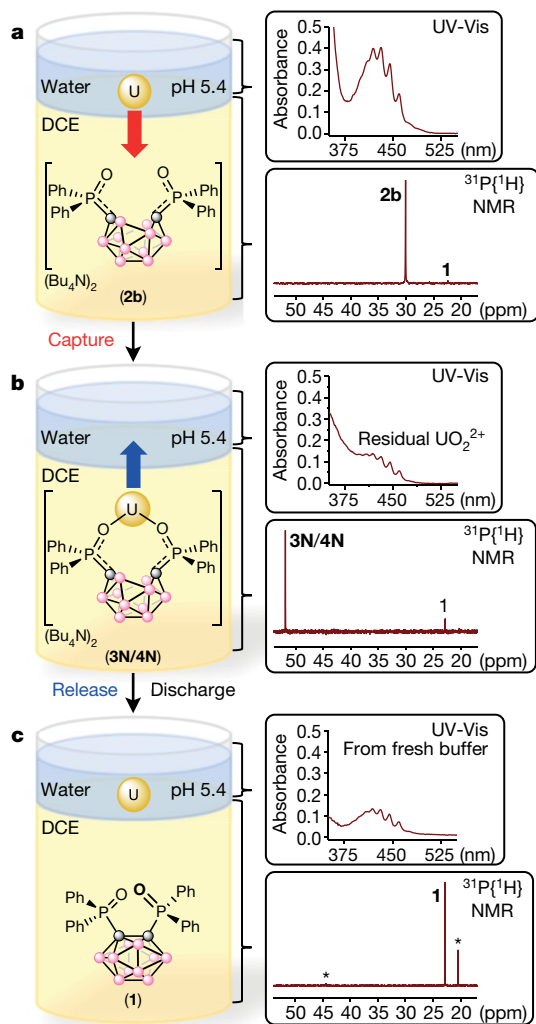


Fig. 3 | Simplified depiction of half-H-cell and spectroscopic measurements for the biphasic electrochemical capture/release of dissolved UO_2^{2+} (yellow sphere) from/to buffered aqueous solutions. See Methods and Extended Data Fig. 7 for an expanded stepwise figure and all experimental details. **a**, Biphasic mixture of UO_2X_2 dissolved in a NaOAc-buffered aqueous solution (pH 5.4) and of electrochemically generated **2b** from **1** ($\text{X} = \text{OAc}^-$ or NO_3^-). Inset, aqueous UV-Vis and organic $^{31}\text{P}\{^1\text{H}\}$ NMR spectra after reduction of **1** to **2b**, but before phase mixing. Residual **1** is observed in the latter owing to the set SOC. **b**, Simplified depiction of the captured UO_2X_2 in the form of **3N** and/or **4N**. Inset, aqueous UV-Vis spectrum showing the capture of UO_2X_2 by the **2b**/DCE layer (top); the corresponding $^{31}\text{P}\{^1\text{H}\}$ NMR spectrum of the DCE layer showing the captured major product (**3N/4N**) and minor residual **1** (bottom). **c**, Biphasic release of UO_2X_2 from the DCE layer to a fresh NaOAc-buffered solution (pH 5.4), following electrochemical oxidation of **3N/4N**. Inset, aqueous UV-Vis and organic $^{31}\text{P}\{^1\text{H}\}$ NMR spectra of free UO_2X_2 and **1**, respectively—both consistent with the release of captured UO_2X_2 from the DCE to the aqueous phase. A small amount (~20%) of unknown byproducts (marked by asterisks) is also observed in the $^{31}\text{P}\{^1\text{H}\}$ NMR spectrum.

- Kim, J. et al. Recovery of uranium from seawater: a review of current status and future research needs. *Sep. Sci. Technol.* **48**, 367–387 (2013).
- Parker, B. F., Zhang, Z., Rao, L. & Arnold, J. An overview and recent progress in the chemistry of uranium extraction from seawater. *Dalton Trans.* **47**, 639–644 (2018).

- Xiong, L.-p. et al. Efficient capture of actinides from strong acidic solution by hafnium phosphonate frameworks with excellent acid resistance and radiolytic stability. *Chem. Eng. J.* **355**, 159–169 (2019).
- Sun, Q. et al. Bio-inspired nano-traps for uranium extraction from seawater and recovery from nuclear waste. *Nat. Commun.* **9**, 1644 (2018).
- Jang, J.-H., Dempsey, B. A. & Burgos, W. D. A model-based evaluation of sorptive reactivities of hydrous ferric oxide and hematite for $\text{U}(\text{VI})$. *Environ. Sci. Technol.* **41**, 4305–4310 (2007).
- Mellah, A., Chegrouche, S. & Barkat, M. The removal of uranium(VI) from aqueous solutions onto activated carbon: kinetic and thermodynamic investigations. *J. Colloid Interface Sci.* **296**, 434–441 (2006).
- Kim, J. H., Lee, H. I., Yeon, J.-W., Jung, Y. & Kim, J. M. Removal of uranium(VI) from aqueous solutions by nanoporous carbon and its chelating polymer composite. *J. Radioanal. Nucl. Chem.* **286**, 129–133 (2010).
- Mehio, N. et al. Quantifying the binding strength of salicylaldehyde–uranyl complexes relative to competing salicylaldehyde–transition metal ion complexes in aqueous solution: a combined experimental and computational study. *Dalton Trans.* **45**, 9051–9064 (2016).
- Kuo, L.-J. et al. Investigations into the reusability of amidoxime-based polymeric adsorbents for seawater uranium extraction. *Ind. Eng. Chem. Res.* **56**, 11603–11611 (2017).
- Fisher, S. P. et al. Nonclassical applications of closo-carborane anions: from main group chemistry and catalysis to energy storage. *Chem. Rev.* **119**, 8262–8290 (2019).
- Núñez, R., Tarrés, M., Ferrer-Ugalde, A., de Biani, F. F. & Teixidor, F. Electrochemistry and photoluminescence of icosahedral carboranes, boranes, metallocarboranes, and their derivatives. *Chem. Rev.* **116**, 14307–14378 (2016).
- Axtell, J. C., Saleh, L. M. A., Qian, E. A. & Spokoyny, A. M. Synthesis and applications of perfunctionalized boron clusters. *Inorg. Chem.* **57**, 2333–2350 (2018).
- Fisher, S. P., Tomich, A. W., Guo, J. & Lavallo, V. Teaching an old dog new tricks: new directions in fundamental and applied closo-carborane anion chemistry. *Chem. Commun.* **55**, 1684–1701 (2019).
- Grimes, R. N. *Carboranes* 2nd edn (Elsevier Science and Technology, 2011).
- Xie, Z. Advances in the chemistry of metallocarboranes of f-block elements. *Coord. Chem. Rev.* **231**, 23–46 (2002).
- Weber, L. et al. Electrochemical and spectroelectrochemical studies of C-benzodiazaborolyl-ortho-carboranes. *Dalton Trans.* **42**, 2266–2281 (2013).
- Charmant, J. P. H. et al. A simple entry into nido- C_2B_{10} clusters: HCl promoted cleavage of the C–C bond in ortho-carboranyl diphosphines. *Dalton Trans.* **11**, 1409–1411 (2008).
- Deng, L., Cheung, M.-S., Chan, H.-S. & Xie, Z. Reduction of 1,2- $(\text{CH}_2)_n$ -1,2- $\text{C}_2\text{B}_{10}\text{H}_{10}$ by group 1 metals. Effects of bridge length/rigidity on the formation of carborane anions. *Organometallics* **24**, 6244–6249 (2005).
- Popescu, A.-R. et al. Uncommon coordination behaviour of P(S) and P(Se) units when bonded to carboranyl clusters: experimental and computational studies on the oxidation of carboranyl phosphine ligands. *Chem. Eur. J.* **17**, 4429–4443 (2011).
- Sundberg, M. R. et al. Nature of intramolecular interactions in hypercoordinate C-substituted 1,2-dicarba-closo-dodecaboranes with short P...P distances. *Inorg. Chem. Commun.* **10**, 713–716 (2007).
- Bombieri, G., Forsellini, E., Day, J. P. & Azeez, W. I. Crystal and molecular structure of dichlorodioxobis(triphenylphosphine oxide)uranium(VI). *Dalton Trans.* **6**, 677–680 (1978).
- Brightli, M., Fux, P., Lagrange, J. & Lagrange, P. Discussion on the complexing ability of the uranyl ion with several crown ethers and cryptands in water and in propylene carbonate. *Inorg. Chem.* **24**, 80–84 (1985).
- Akono, S. B., Fawcett, J., Holloway, J. H., Russell, D. R. & Leban, I. Structures of cis- and trans-dichlorodioxobis(triphenylphosphine oxide)uranium(VI). *Acta Cryst. C* **47**, 45–48 (1991).
- Bard, A. J. & Faulkner, L. R. *Electrochemical Methods: Fundamentals and Applications* 2nd edn (Wiley, 2000).
- Liu, C. et al. A half-wave rectified alternating current electrochemical method for uranium extraction from seawater. *Nat. Energy* **2**, 17007 (2017).
- Chi, F., Zhang, S., Wen, J., Xiong, J. & Hu, S. Highly efficient recovery of uranium from seawater using an electrochemical approach. *Ind. Eng. Chem. Res.* **57**, 8078–8084 (2018).
- Paiva, A. P. & Malik, P. Recent advances on the chemistry of solvent extraction applied to the reprocessing of spent nuclear fuels and radioactive wastes. *J. Radioanal. Nucl. Chem.* **261**, 485–496 (2004).
- Hunt, C., Mattejat, M., Anderson, C., Sepunaru, L. & Ménard, G. Symmetric phthalocyanine charge carrier for dual redox flow battery/capacitor applications. *ACS Appl. Energy Mater.* **2**, 5391–5396 (2019).
- Quilès, F., Nguyen-Trung, C., Carteret, C. & Humbert, B. Hydrolysis of uranyl(VI) in acidic and basic aqueous solutions using a noncomplexing organic base: a multivariate spectroscopic and statistical study. *Inorg. Chem.* **50**, 2811–2823 (2011).
- Pant, D. D. & Khandelwal, D. P. The absorption and fluorescence spectra of uranyl nitrate solutions at room temperature. *P. Indian Acad. Sci. A* **50**, 323–335 (1959).

Publisher's note Springer Nature remains neutral with regard to jurisdictional claims in published maps and institutional affiliations.

© The Author(s), under exclusive licence to Springer Nature Limited 2020

Methods

General considerations

All manipulations were performed under an atmosphere of dry, oxygen-free N₂ or Ar by means of standard Schlenk or glovebox techniques (MBraun equipped with a -38 °C freezer, or VAC gloveboxes). Hexanes, pentane, DCM and benzene were dried on an MBraun solvent purification system. Acetonitrile (-H₃ and -D₃) was dried over CaH₂ for several days before distillation. THF was dried over sodium benzophenone and distilled. PC was degassed by freeze-pump-thaw cycles and stored on activated 4-Å molecular sieves before use. DCE was initially distilled, followed by drying over CaH₂ for several days before a second distillation and subsequent storage on activated 4-Å molecular sieves. [FeCp₂][PF₆], [Bu₄N][Cl] and TPO were purchased from Fisher Scientific; trimethylphosphine (Mes₃P) was purchased from VWR International; *n*BuLi (1.6 M in hexanes) was purchased from Sigma Aldrich; all were used without further purification. *Ortho*-carborane was purchased from Boron Specialties and sublimed before use. Ph₂PCl was purchased from Sigma Aldrich and vacuum-distilled before use. CoCp₂ was purchased from Sigma Aldrich and purified by filtration through celite using pentane, followed by recrystallization from pentane at -38 °C over several days. [Bu₄N][PF₆] was purchased from Oakwood Chemicals and purified by twice recrystallizing from hot ethanol. The recrystallized product was then washed with cold water, cold ethanol and pentane before drying at 100 °C under vacuum for 24 h. Sodium acetate (NaOAc) buffer was prepared from a stock solution purchased from Sigma Aldrich (pH 4.9) and adjusted to pH 5.4 using NaOH. The pH value was confirmed using a pH meter. Ketjenblack EC-600JD was purchased from a private supplier. UO₂Cl₂(TPO)₂ (ref. ²¹), [UO₂Cl₂(THF)₂]₂ (ref. ³¹), [UO₂(NO₃)₂(THF)₃] (ref. ³²), K₂C₈ (ref. ³³) and bis(triphenylphosphoranylidene)ammonium hexafluorophosphate ([Ph₃PNPPPh₃][PF₆]) (ref. ³⁴) were prepared by procedures reported in the literature.

NMR. NMR spectra were obtained using a Varian Unity Inova 500 MHz or Agilent Technologies 400 MHz spectrometer, and were referenced to residual solvent resonances of acetonitrile (MeCN-d₃) or dichloromethane (DCM-d₂) or externally (¹¹B, 85% (Et₂O)BF₃·³¹P, 85% H₃PO₄). Chemical shifts (δ) were recorded in parts per million. All ¹¹B NMR spectra were processed using MestReNova software to reduce a background signal with a linewidth of approximately 3,000 Hz from the Pyrex NMR tubes. The NMR time-domain data were first left-shifted to discard the first -0.1 ms. To correct the linear phase change, a linear prediction was used to fill the initial discarded data before the Fourier transform or an appropriate linear phase correction was applied to the frequency-domain data after the Fourier transform. The relaxation times T₁ for ³¹P nuclei were determined using the inversion recovery method. The delay times after the 180° inversion pulse were varied up to the maximum of five times of the expected T₁ values. The signal recovery curve was fitted with an exponential function to extract the T₁ values. Subsequent one-dimensional spectra were acquired with five times the longest T₁ value measured for accurate integrations (where T₁ values were determined for TPO: 2.3 s; Mes₃P: 5.1 s; [Ph₃PNPPPh₃][PF₆]: 7.1 s; **1**: 0.51 s; **3**: 0.64 s; and **4**: 0.57 s).

UV-Vis. UV-Vis absorption spectra were collected using a Shimadzu UV-2401PC spectrophotometer. The UO₂²⁺ extinction coefficient (ε) was experimentally determined to be 7.715 litres mol⁻¹ cm⁻¹ (460 nm) at pH 5.4.

Elemental analyses. Elemental analyses (C, N, H) were performed at the University of California, Berkeley using a Perkin Elmer 2400 Series II combustion analyser.

Cyclic voltammetry. Cyclic voltammetry was performed using a CH Instruments Electrochemical Analysis potentiostat, equipped with a

3-mm-diameter glassy carbon working electrode, a Ag-wire pseudo-reference electrode and a Pt-wire counter electrode using a [Bu₄N][PF₆] (0.1 M) solution as the supporting electrolyte. Cyclic voltammograms were referenced to the Fc/Fc⁺ redox couple.

Galvanostatic bulk electrolysis. Galvanostatic bulk electrolysis cycling experiments were carried out inside an Ar glovebox using a Metrohm Autolab PGSTAT128N potentiostat/galvanostat. The full experimental setups for both the mono- and biphasic cycling experiments are described in sections 'Monophasic electrochemical capture and release of UO₂²⁺' and 'Biphasic electrochemical capture and release of UO₂²⁺'.

X-ray crystallography. X-ray crystallography data were collected on a Bruker KAPPA APEX II diffractometer equipped with an APEX II CCD detector using a TRIUMPH monochromator with a Mo Kα X-ray source (wavelength α = 0.71073 Å). The crystals were mounted on a cryoloop under Paratone-N oil, and all data were collected at 100(2) K using an Oxford nitrogen-gas cryostream system. A hemisphere of data was collected using ω scans with 0.5° frame widths (ω, angle between the X-ray source and the sample). Data collection and cell-parameter determination were conducted using the SMART program. Integration of the data frames and refinement of the final cell parameters were performed using SAINT software. Absorption correction of the data was carried out using SADABS. Structure determination was done using direct or Patterson methods and difference Fourier techniques. All hydrogen atom positions were idealized and rode on the atom of attachment. Structure solution, refinement, graphics and creation of publication materials were performed using SHELXTL or OLEX².

Synthesis of closo-(1,2-(Ph₂PO)₂-1,2-C₂B₁₀H₁₀) (1). The synthesis of compound **1** was accomplished in two steps by modifications to literature procedures^{19,35}.

Step 1. A solution of *n*BuLi in hexane (1.6 M, 28.2 ml, 45 mmol) was added dropwise to a solution of *ortho*-carborane (3.1 g, 21.5 mmol) in dry diethyl ether (250 ml) at -78 °C, resulting in the formation of a fine colourless precipitate. The reaction was slowly warmed to room temperature. After stirring for 30 min at room temperature, the mixture was cooled to 0 °C, and Ph₂PCl (7.7 ml, 41.7 mmol) was added dropwise, resulting in a pale orange solution with a colourless precipitate. The mixture was stirred for 30 min at 0 °C. The solution was brought to room temperature and stirred for 30 min and was subsequently warmed to reflux and stirred for an additional 30 min. The solution was cooled to 0 °C, and water (30 ml) was slowly added to the mixture. The mixture was allowed to stir for 20 min and was filtered over a glass frit, where the resulting solid was washed with additional water (30 ml) and diethyl ether (20 ml). The solid was dried under vacuum at 100 °C for 2 h. The product was recrystallized from a mixture of hexane/toluene and was obtained in 81% yield (8.6 g, 16.7 mmol) ¹H NMR (400 MHz, CDCl₃): δ 7.06–7.47 (m, 20H); 0.98–2.66 (broad, 10H). ¹¹B NMR (400 MHz, CDCl₃): δ -0.40, -9.42. ¹¹B{¹H} NMR (400 MHz, CDCl₃): δ -0.40, -7.21, -9.42. ³¹P{¹H} NMR (400 MHz, CDCl₃): δ 7.88.

Step 2. A solution of H₂O₂ (30% in water, 1.8 ml, 58.7 mmol) was added dropwise to a solution of [closo-(1,2-(Ph₂P)₂-1,2-C₂B₁₀H₁₀)] (from step 1) (2.1 g, 4.1 mmol) in THF (50 ml). The reaction was stirred for 3 h at room temperature. The reaction was monitored by ³¹P NMR for formation of an unwanted side-product at 49 ppm. Once this product formed, the reaction was discontinued by addition of chloroform. The mixture was washed with water and brine, the phases were separated and the organic layer was dried with Na₂SO₄. The solvent was removed, and the solid was slowly recrystallized from acetonitrile to yield a colourless crystalline solid. The solid was dried under vacuum at 80 °C for several hours (1.4 g, 2.6 mmol, 60% yield). Single crystals suitable for X-ray crystallography were obtained by vapour diffusion of pentane in a saturated THF solution of **1**. ¹H NMR (400 MHz, MeCN-d₃): δ 7.99 (m, 8H),

7.63 (m, 4H), 7.54 (m, 8H), 2.5 (broad s, 10H). ^{11}B and $^{11}\text{B}\{^1\text{H}\}$ NMR (400 MHz, MeCN-d_3): δ 0.66, -8.75. $^{31}\text{P}\{^1\text{H}\}$ NMR (400 MHz, MeCN-d_3): δ 22.8. Anal. calc. for $\text{C}_{26}\text{H}_{30}\text{B}_{10}\text{O}_2\text{P}_2$: C, 57.35; H, 5.55. Found: C, 57.33; H, 5.66. Selected interatomic distances for **1** were C...C: 1.688(4) Å, P...P: 3.537 Å.

Synthesis of $\text{UO}_2\text{Cl}_2(\mathbf{1})_2$. A 20-ml vial equipped with a magnetic stirbar was charged with **1** (54.4 mg, 0.1 mmol) and 2 ml of DCM. In a separate vial, $[\text{UO}_2\text{Cl}_2(\text{THF})_2]_2$ (24.2 mg, 0.025 mmol) was dissolved in 2 ml of DCM and added to the stirring solution of **1**, resulting in the formation of a light-yellow suspension. After 1 h, the reaction mixture became homogeneous. This was stirred for an additional 24 h at room temperature. The solvent was removed, yielding a yellow solid (62.5 mg). Multiple attempts were made to obtain single crystals suitable for XRD studies, but failed. ^1H NMR (400 MHz, DCM-d_2): δ 8.32–6.29 (m, 20H), 2.5 (broad s, 10H). ^{11}B and $^{11}\text{B}\{^1\text{H}\}$ NMR (400 MHz, DCM-d_2): δ 5.84, -8.46. $^{31}\text{P}\{^1\text{H}\}$ NMR (400 MHz, DCM-d_2): δ 38.8 (s), 38.4 (s). Anal. calc. for $\text{C}_{52}\text{H}_{60}\text{B}_{20}\text{Cl}_2\text{O}_6\text{P}_4\text{U}\cdot 1/2\text{CH}_2\text{Cl}_2$: C, 43.05; H, 4.16. Found: C, 42.76; H, 4.32.

Synthesis of $[\text{CoCp}^*_2]_2[\text{UO}_2\text{Cl}_2(\text{nido-1,2-(Ph}_2\text{PO)}_2-1,2-\text{C}_2\text{B}_{10}\text{H}_{10})]$ (2a**).** A 20-ml vial equipped with a magnetic stirbar was charged with **1** (54.4 mg, 0.1 mmol) and 6 ml of benzene. In a separate vial, CoCp^*_2 (69.1 mg, 0.2 mmol, 2.0 equiv.) was dissolved in 4 ml of benzene and added dropwise to the stirring solution of **1**. Upon addition, a yellow solid immediately precipitated from the reaction mixture, and the mixture was stirred for an additional 4 h at room temperature. Stirring was discontinued and the solid was allowed to settle to the bottom of the vial. The supernatant was decanted and filtered on a plug of celite. The solids were washed with benzene (3 × 6 ml) and each washing was filtered over the same celite plug. The remaining solids were then dissolved in a minimal amount of MeCN (2 ml) and filtered on the same celite plug into a new vial. The MeCN filtrate was collected and the volatiles were removed in vacuo, yielding a shiny golden-yellow solid (114.3 mg, 0.95 mmol, 95% yield). Single crystals suitable for X-ray crystallography were obtained by vapour diffusion of Et_2O in a saturated MeCN solution of **2a** at -38 °C. ^1H NMR (400 MHz, MeCN-d_3): δ 8.05 (broad m, 8H), 7.24 (broad s, 12H), 1.62 (s, 60H). We note that carborane B–H resonances were too broad to be observed. ^{11}B and $^{11}\text{B}\{^1\text{H}\}$ NMR (400 MHz, MeCN-d_3): δ 20.24, -0.62, -18.46, -22.06. $^{31}\text{P}\{^1\text{H}\}$ NMR (400 MHz, MeCN-d_3): δ 29.8. Anal. calc. for $\text{C}_{66}\text{H}_{90}\text{B}_{10}\text{Co}_2\text{O}_2\text{P}_2$: C, 65.88; H, 7.54. Found: C, 65.57; H, 7.67. Selected interatomic distances for **2a** were C...C: 2.860 Å, P...P: 5.036 Å.

Synthesis of $[\text{Bu}_4\text{N}]_2[(\text{nido-1,2-(Ph}_2\text{PO)}_2-1,2-\text{C}_2\text{B}_{10}\text{H}_{10})]$ (2b**).** The synthesis of compound **2b** was accomplished in two steps.

Step 1. In the glovebox, a 250-ml round-bottom flask equipped with a magnetic stirbar was charged with **1** (272.2 mg, 0.5 mmol) and 20 ml of THF, and cooled to -78 °C. In a separate vial, KC_8 (182.4 mg, 1.35 mmol, 2.7 equiv.) was suspended in 20 ml of THF and added slowly dropwise to the stirring solution of **1**. Upon addition, the KC_8 suspension began to turn grey, and was stirred for 30 min at room temperature. Stirring was discontinued and the mixture was filtered over a pad of celite on a fine glass frit. The graphite pad was washed additionally with MeCN (3 × 5 ml). The filtrate was collected and the volatiles were removed in vacuo, yielding a pale-yellow oil. The oil was redissolved in THF (5 ml) and layered with 5 ml of pentane, and was recrystallized at -38 °C, yielding a white solid (234.1 mg, 0.38 mmol, 75% yield). ^1H NMR (400 MHz, MeCN-d_3): δ 7.81 (broad m, 8H), 7.28 (broad m, 12H). Carborane B–H resonances were too broad to be observed. ^{11}B NMR (400 MHz, MeCN-d_3): δ 20.24, -0.62, -18.46, -22.06. $^{31}\text{P}\{^1\text{H}\}$ NMR (400 MHz, MeCN-d_3): δ 31.8. Anal. calc. for $\text{C}_{26}\text{H}_{30}\text{B}_{10}\text{K}_2\text{O}_2\text{P}_2\cdot\text{THF}$: C, 51.86; H, 5.51. Found: C, 51.09; H, 5.47.

Step 2. A 20-ml vial equipped with a magnetic stirbar was charged with $[\text{K}]_2[(\text{nido-1,2-(Ph}_2\text{PO)}_2-1,2-\text{C}_2\text{B}_{10}\text{H}_{10})\cdot\text{THF}]$ (655.4 mg, 0.94 mmol) (Step 1) and 15 ml of DCM, and was cooled to -78 °C. In a separate vial,

$[\text{Bu}_4\text{N}][\text{Cl}]$ (528 mg, 1.88 mmol, 2.0 equiv.) was dissolved in 10 ml of DCM and added dropwise to the stirring carborane suspension. Upon addition, the reaction mixture became homogenous, and after 1 h a white precipitate began to settle. This mixture was stirred for 2 h at room temperature. Stirring was discontinued and all volatiles were removed, yielding a pale-yellow solid. A minimal amount of DCM (3 ml) was added and the mixture was filtered on a celite plug. The solids were washed with chilled DCM (3 × 2 ml) and each washing was filtered over the same celite plug. The DCM filtrate was collected and the volatiles were removed in vacuo, yielding a pale-yellow residue; this was triturated with pentane (10 ml) and dried in vacuo to yield an off-white solid, which was recrystallized from DCM and pentane (690.4 mg, 0.67 mmol, 71% yield). ^1H NMR (400 MHz, MeCN-d_3): δ 8.03 (m, 8H), 7.25 (broad s, 12H), 3.08 (m, 16H), 1.59 (m, 16H), 1.35 (m, 16H), 0.96 (t, 24H). Carborane B–H resonances were too broad to be observed. ^{11}B and $^{11}\text{B}\{^1\text{H}\}$ NMR (400 MHz, MeCN-d_3): δ 20.25, -0.65, -18.42, -22.05. $^{31}\text{P}\{^1\text{H}\}$ NMR (400 MHz, MeCN-d_3): δ 30.1. Anal. calc. for $\text{C}_{58}\text{H}_{102}\text{B}_{10}\text{N}_2\text{O}_2\text{P}_2$: C, 67.67; H, 9.99. Found: C, 66.81; H, 10.29.

Synthesis of $[\text{CoCp}^*_2]_2[\text{UO}_2\text{Cl}_2(\text{nido-1,2-(Ph}_2\text{PO)}_2-1,2-\text{C}_2\text{B}_{10}\text{H}_{10})]$ (3**).** A 20-ml vial equipped with a magnetic stirbar was charged with $[\text{UO}_2\text{Cl}_2(\text{THF})_2]_2$ (16.9 mg, 0.018 mmol) and 4 ml of MeCN. In a separate vial, **2a** (42.2 mg, 0.035 mmol) was dissolved in 4 ml of MeCN and then added dropwise to the stirring solution of $[\text{UO}_2\text{Cl}_2(\text{THF})_2]_2$, turning dark yellow. After stirring for 5 min, a yellow solid began to precipitate from the reaction mixture, and this was stirred at room temperature for 4 h. Stirring was discontinued and the mixture was passed over a celite plug, collecting a yellow solid and a yellow filtrate. The solvent was removed from the yellow filtrate, yielding a yellow solid, which was washed with THF (3 × 2 ml) and passed over another celite plug. The filtrate was collected and the volatiles were removed in vacuo, yielding a yellow powder. Residual $[\text{CoCp}^*_2][\text{Cl}]$ was removed by selectively recrystallizing the mixture from pyridine/ Et_2O at -38 °C. The supernatant was transferred and the volatiles were removed, collecting a yellow solid (36.3 mg, 0.024 mmol, 69% yield). Single crystals suitable for XRD studies were grown by vapour diffusion of Et_2O into a saturated MeCN solution of **3** at room temperature. ^1H NMR (400 MHz, MeCN-d_3): δ 8.13 (m, 10H), 7.35 (m, 10H), 1.66 (s, 60H). Carborane B–H resonances were too broad to be observed. ^{11}B and $^{11}\text{B}\{^1\text{H}\}$ NMR (400 MHz, MeCN-d_3): δ 0.27, -16.90, -19.69. $^{31}\text{P}\{^1\text{H}\}$ NMR (400 MHz, MeCN-d_3): δ 51.12. Anal. calc. for $\text{C}_{66}\text{H}_{90}\text{B}_{10}\text{Cl}_2\text{Co}_2\text{O}_4\text{P}_2\text{U}\cdot 2\text{MeCN}$: C, 51.70; H, 5.95; N, 1.72. Found: C, 51.91; H, 5.88; N, 1.74. Selected interatomic distances and angles for **3** were C...C: 2.855 Å; P...P: 4.697 Å; O1–U–O2: 86.5°(3°).

Synthesis of $[\text{CoCp}^*_2]_2[\text{UO}_2(\text{nido-1,2-(Ph}_2\text{PO)}_2-1,2-\text{C}_2\text{B}_{10}\text{H}_{10})_2]$ (4**).** A 20-ml vial equipped with a magnetic stirbar was charged with **2a** (26.6 mg, 0.022 mmol) and 1.5 ml of MeCN. In a separate vial, $[\text{UO}_2\text{Cl}_2(\text{THF})_2]_2$ (5.3 mg, 0.0055 mmol) was dissolved in 1.5 ml of MeCN and then added dropwise to the stirring solution of **2a**. After stirring for 5 min, a yellow solid began to precipitate from the reaction mixture, and this was stirred at room temperature for 24 h. Stirring was discontinued and the solid was allowed to settle to the bottom of the vial. The supernatant was decanted and filtered on a celite plug. The solids were washed with MeCN (3 × 2 ml) and each washing was filtered over the same celite plug. The remaining solids were then dissolved in a minimal amount of pyridine and filtered on the same celite plug into a new vial. The pyridine filtrate was collected and the volatiles were removed in vacuo, yielding a light-yellow powder (35.5 mg, 0.018 mmol, 80% yield). Single crystals suitable for XRD analysis were grown from a small-scale reaction in a J. Young NMR tube, which was charged with a solution of **2a** (12.0 mg, 0.01 mmol) in MeCN-d_3 (0.25 ml). A solution of $[\text{UO}_2\text{Cl}_2(\text{THF})_2]_2$ (2.4 mg, 0.0025 mmol) in MeCN-d_3 (0.25 ml) was added to this, whereupon crystals suitable for XRD analysis slowly formed on the walls of the NMR tube. ^1H NMR (400 MHz, MeCN-d_3): δ 8.13 (m, 15H), 7.38 (m, 10H), 7.24 (m, 15H), 1.68 (s, 60H). Carborane B–H

resonances were too broad to be observed. ^{11}B and $^{11}\text{B}\{\text{H}\}$ NMR (400 MHz, MeCN-d_3): δ 0.26, -17.15, -20.66. $^{31}\text{P}\{\text{H}\}$ NMR (400 MHz, MeCN-d_3): δ 52.0. Anal. calc. for $\text{C}_{97}\text{H}_{120}\text{B}_{20}\text{Co}_2\text{O}_6\text{P}_4\text{U}$: C, 54.76; H, 5.99. Found: C, 55.22; H, 6.36. Selected interatomic distances and angles for **4** were C...C: 2.857 Å; P...P: 4.806 Å; O1-U-O2: 89.7° (17°).

Chemical capture and release of UO_2^{2+}

Formation of in situ generated $[(\text{UO}_2)(\text{TPO})_2\text{Cl}_2]$. A 20-ml vial equipped with a magnetic stirbar was charged with **1** (2.0 equiv., 5.4 mg, 0.01 mmol), TPO (4.0 equiv., 5.6 mg, 0.02 mmol) and Mes_3P (4.0 equiv., 7.7 mg, 0.02 mmol) and dissolved in a 3:1 PC:benzene (3 ml) solvent system. A 500- μl aliquot was taken from this mixture and placed in an NMR tube equipped with a MeCN-d_3 capillary tube. A $^{31}\text{P}\{\text{H}\}$ NMR spectrum was collected and the relative integrations were recorded (Extended Data Fig. 5a). The NMR solution was returned to the vial and $[\text{UO}_2\text{Cl}_2(\text{THF})_2]$ (0.5 equiv., 2.4 mg, 0.0025 mmol) was added. The mixture was stirred vigorously until all the solids were dissolved (~20 min), resulting in a light-yellow coloured solution. After 1 h, a 500- μl aliquot was taken from the reaction mixture and placed in an NMR tube equipped with a MeCN-d_3 capillary tube. A $^{31}\text{P}\{\text{H}\}$ NMR spectrum was obtained (Extended Data Fig. 5b). After the spectrum was recorded, the NMR sample was transferred back into the reaction mixture.

Reduction. CoCp_2^+ (4.0 equiv., 6.6 mg, 0.02 mmol) in 100 μl of benzene was added dropwise to the generated solution described above. Upon addition, the solution turned golden in colour and was stirred for 1 h at room temperature. A 500- μl aliquot was then taken from the reaction mixture and placed in an NMR tube equipped with a MeCN-d_3 capillary tube. A $^{31}\text{P}\{\text{H}\}$ NMR spectrum was obtained (Extended Data Fig. 5c), and then the NMR solution was transferred back into the reaction mixture.

Oxidation. $[\text{Fc}][\text{PF}_6]$ (4.0 equiv, 6.6 mg, 0.02 mmol) was added to the reduced solution described above. Upon addition, the solution turned green and then a golden colour. The solution was stirred for 1 h at room temperature, after which a 500- μl aliquot was taken from the reaction mixture and placed in an NMR tube equipped with a MeCN-d_3 capillary tube. A $^{31}\text{P}\{\text{H}\}$ NMR spectrum was obtained (Extended Data Fig. 5d). After the spectrum was obtained, the NMR sample was transferred back into the reaction mixture.

Monophasic electrochemical capture and release of UO_2^{2+}

Experimental conditions. Galvanostatic bulk electrolysis experiments were carried out in a divided glass H-cell (Extended Data Fig. 8a, b). The physical barrier between each component of the cell and the respective two Bio-Logic high-surface coiled Pt electrodes was an anion-exchange membrane (Membranes International, AMI-7001) held in place by two fluorinated ethylene propylene-encapsulated silicon o-rings with a metal clamp. The electrodes were cleaned by rinsing with distilled water and acetone and then heating until white-hot with a butane torch before use. The anion-exchange membrane was soaked in a 0.1 M $[\text{Bu}_4\text{N}][\text{PF}_6]$ solution of PC/benzene (3:1) over 3-Å molecular sieves for 24 h before use. The left compartment, containing the counter electrode, consisted of Fc (41.9 mg, 0.225 mmol) and $[\text{Fc}][\text{PF}_6]$ (74.5 mg, 0.225 mmol) in 7.0 ml of a 0.1 M $[\text{Bu}_4\text{N}][\text{PF}_6]$ PC:benzene solution. The right compartment, containing the working electrode, contained **1** (5 equiv., 40.8 mg, 0.075 mmol), TPO (6 equiv., 25.0 mg, 0.09 mmol), $[\text{UO}_2\text{Cl}_2(\text{THF})_2]$ (0.5 equiv., 7.3 mg, 0.0075 mmol of dimer (1.0 equiv. of U monomer)) and $[\text{Ph}_3\text{PNPPh}_3][\text{PF}_6]$ (1.0 equiv., 10.2 mg, 0.015 mmol) in a 0.1 M $[\text{Bu}_4\text{N}][\text{PF}_6]$ PC:benzene solution (7.0 ml).

Experimental parameters. The cell was charged/discharged over the course of six cycles. To initiate UO_2^{2+} capture, the first cycle was charged with an applied current of -201.0 μA over the course of 6 h to a 75% SOC relative to the $[\text{UO}_2\text{Cl}_2(\text{THF})_2]$ concentration. After the cell was charged,

a wait period of 2 h was incorporated between charge/discharge cycles (Fig. 2c, grey dashed). UO_2^{2+} release was achieved by discharging the cell galvanostatically at an applied current of 68.94 μA over the course of 13 h, using voltage cutoffs (0.0 V), to a final SOC of approximately 15% relative to the initial $[\text{UO}_2\text{Cl}_2(\text{THF})_2]$ concentration. After each cell discharge, a wait period of 4–5 h was incorporated (depending on when the voltage cutoffs were applied) between discharging/charging cycles. Each additional cycle thereafter was charged and discharged galvanostatically at currents of -160.87 μA and 68.94 μA , respectively. This resulted in charging cycles of -15–75% SOC and -75–15% SOC, respectively. Between each charge/discharge a $^{31}\text{P}\{\text{H}\}$ NMR spectrum was obtained (Extended Data Fig. 6a) using a 40-s relaxation delay (see NMR details above) with $[\text{Ph}_3\text{PNPPh}_3][\text{PF}_6]$ as the standard. We note that an excess of **1** was used to keep the applied current (I_{app}) below the limiting current at any given time ($I_l(t)$) for the presumed electrochemical-chemical mechanism involving reduction of **1** followed by uranyl ligation. This allowed the use of a galvanostatic charge/discharge procedure operating close to the mass-transfer-controlled plateau (similar to potentiostatic methods) but with the added benefit of not requiring prior knowledge of the optimal applied voltage, which is a function of both the onset of the reductive process and the total cell impedance²⁴. Attempts at GBE with stoichiometric equivalents of **1** revealed an earlier-than-expected onset of $I_{\text{app}} > I_l(t)$, clearly indicating that additional and unwanted electrochemical processes were being accessed and perhaps suggesting an initial degradation of **1** within the system. Therefore, an initial ratio of 0.5:6:8 for $[\text{UO}_2\text{Cl}_2(\text{THF})_2]$:**1**:TPO reagents was used.

Biphasic electrochemical capture and release of UO_2^{2+}

Experimental conditions. A complete, stepwise, half-cell figure of the experiments conducted in this section, along with spectroscopic data, are shown in Extended Data Fig. 7. Two-electrode galvanostatic bulk electrolysis was performed in an argon glovebox using a two-compartment H-cell with a glass-frit separator, a stir bar in each compartment, and reticulated vitreous carbon (RVC) foam electrodes for both the working and counter electrodes (Extended Data Fig. 8c, d). The RVC foam electrodes consisted of a -5-cm steel rod inserted into a 100 PPI Duocel RVC foam core (length -2.5 cm; diameter -3 mm), with a tap bore (length -5 mm; diameter -2 mm), which was filled with molten gallium to fuse the steel connector to the RVC foam. Each electrode had an end-to-tip resistance of <5 Ω . The RVC electrodes were rinsed with methanol and dried under reduced pressure overnight before use. The Ketjenblack used was dried for 48 h in a 175 °C oven and ground in a glass mortar and pestle under inert atmosphere before use.

Reduction (charging). The counter compartment consisted of 400 mg of Ketjenblack suspended in 6 ml of a 0.1 M solution of $[\text{Bu}_4\text{N}][\text{PF}_6]$ in DCE. The working compartment consisted of **1** (34 mg, 0.0625 mmol, 1.0 equiv.) dissolved in 6 ml of a 0.1 M solution of $[\text{Bu}_4\text{N}][\text{PF}_6]$ in DCE. A charging current of -107.1 μA with a -9.25 C charge cutoff was used, resulting in a -75% SOC after 24 h assuming 100% Coulombic efficiency. Upon completion, the working compartment solution was analysed by $^{31}\text{P}\{\text{H}\}$ NMR spectroscopy to reveal the formation of **2b** (Extended Data Fig. 9a). The working compartment solution was then removed from the H-cell and placed in a 20-ml vial for subsequent capture chemistry.

UO_2^{2+} capture. A 5-ml vial was charged with excess $\text{UO}_2(\text{NO}_3)_2(\text{THF})_2$ (42 mg, 0.078 mmol, 1.25 equiv.) and dissolved in 3 ml of a 0.1 M sodium acetate buffer adjusted to pH 5.4 (0.026 M UO_2^{2+}). An aliquot of the resulting pale-yellow solution was used to record an initial UV-Vis spectrum (Extended Data Fig. 10a, blue). The aliquot was transferred back to the 5-ml vial and this solution was added slowly, dropwise and without stirring to the DCE solution containing the electrochemically reduced **1** (forming **2b**). After addition, the mixture was allowed to stir for 2 h, resulting in a bright-yellow organic phase and a very-pale-yellow

aqueous phase. Stirring was discontinued and the organic and aqueous phases were separated using a small separatory funnel. An aliquot of the aqueous phase was used to record a UV-Vis spectrum (Extended Data Fig. 10a, red), indicating that 0.022 mmol of UO_2^{2+} remained, which is equivalent to the capture of 0.056 mmol (-0.9 equiv.) to the organic phase. A 1-ml aliquot was taken from the pale-yellow dichloroethane layer and transferred to an NMR tube. An unlocked $^{31}\text{P}\{\text{H}\}$ NMR spectrum was collected indicating the formation of **3N/4N** (Extended Data Fig. 9b). The NMR solution was returned to the 20-ml vial.

Oxidation (discharging). Two-electrode galvanostatic bulk electrolysis (discharging) of the captured DCE solution was performed using the same cell used for charging. A discharging current of 107.1 μA was applied until 9.49 C of charge was transferred, resulting in a final SOC of -0% (assuming 100% Coulombic efficiency and no loss of material during the biphasic capture). Upon completion, the working compartment solution was removed and placed in a 20-ml vial for subsequent release chemistry.

UO_2^{2+} release. The 20-ml vial containing the electrochemically oxidized **3N/4N** yellow DCE solution was equipped with a stirbar, and a solution of 0.1 M sodium acetate buffer adjusted to pH 5.4 (3 ml) was added dropwise. The mixture was allowed to stir for 12 h, resulting in a pale-yellow aqueous phase and a colourless organic layer. The organic and aqueous phases were separated using a small separatory funnel, and an aliquot of the aqueous layer was used to take a UV-Vis spectrum indicating the presence of released UO_2^{2+} (0.031 mmol, -0.5 equiv.) (Extended Data Fig. 10b). A 1-ml aliquot was taken from the yellow DCE layer and transferred to an NMR tube. An unlocked $^{31}\text{P}\{\text{H}\}$ NMR spectrum was collected that indicated the clean formation of **1** and a small unknown byproduct at 20.1 ppm (Extended Data Fig. 9c).

Biphasic control experiments

UO_2^{2+} migration from water to DCE in the absence of carborane (1** or **2a/b**).** A 5-ml vial was charged with $\text{UO}_2(\text{NO}_3)_2(\text{THF})_2$ (14.0 mg, 0.026 mmol) and dissolved in 1.5 ml of a 0.1 M sodium acetate buffer adjusted to pH 5.4 (0.017 M UO_2^{2+}). An aliquot of the resulting pale-yellow solution was used to record an initial UV-Vis spectrum (Extended Data Fig. 10c, blue). The aliquot was transferred back to the 5-ml vial. A separate 20-ml vial equipped with a stirbar was charged with $[\text{Bu}_4\text{N}][\text{PF}_6]$ (0.2324 g, 0.1 M) dissolved in DCE (6.0 ml). To the clear DCE solution, the pale-yellow aqueous solution was added slowly dropwise over the course of 2 min without stirring. After addition, the mixture was allowed to stir for 4 h and the organic phase remained clear. Stirring was discontinued and the organic and aqueous phases were separated using a small separatory funnel. Small aliquots of the aqueous (Extended Data Fig. 10c, red) and organic (Extended Data Fig. 10d) phases were used to record UV-Vis spectra, which together clearly indicated that the UO_2^{2+} had remained in the aqueous phase.

UO_2^{2+} migration from water to DCE in the presence of **1.** A 5-ml vial was charged with $\text{UO}_2(\text{NO}_3)_2(\text{THF})_2$ (14.0 mg, 0.026 mmol, 1.0 equiv.) dissolved in 1.5 ml of a 0.1 M sodium acetate buffer adjusted to pH 5.4 (0.017 M UO_2^{2+}). An aliquot of the resulting pale-yellow solution was used to record an initial UV-Vis spectrum (Extended Data Fig. 10e, blue). The aliquot was transferred back to the 5-ml vial. A separate 20-ml vial with a stirbar was charged with **1** (14.1 mg, 0.026 mmol, 1.0 equiv.), $[\text{Bu}_4\text{N}][\text{PF}_6]$ (0.2324 g, 0.1 M) and DCE (6.0 ml). To the clear DCE solution, the pale-yellow aqueous solution was added slowly dropwise over the course of 2 min without stirring. After addition, the mixture was allowed to stir for 3 h and the organic phase remained clear. Stirring was discontinued and the organic and aqueous phases were separated using a small separatory funnel. Small aliquots of the aqueous (Extended Data Fig. 10e, red) and organic (Extended Data Fig. 10f) phases were used to record UV-Vis spectra, which together clearly indicated negligible transfer of UO_2^{2+} from the aqueous to the organic phase.

DFT studies

DFT calculations were performed using Gaussian 09.2³⁶. Geometry optimizations for all molecules were performed using the B3LYP/def2-SVP^{37,38} level of theory (see Supplementary Information for atom coordinates) in DCM using the conductor-like polarizable continuum model (CPCM) implemented in the Gaussian 09 software^{39–41}. Electron density surfaces with electrostatic potentials were extracted from optimized **1** and **2a** (Extended Data Fig. 1d). Thermal energy corrections were extracted from the results of the frequency analyses performed at the same level of theory. Frequency analyses of all molecules and intermediates contained no imaginary frequency, showing that these are energy minima. The equilibrium constants were calculated from the Gibbs free energy values G for the proton-transfer reactions ($K_{\text{eq}} = e^{-\Delta G/(RT)}$; R , molar gas constant; T , temperature). See Supplementary Information for the competition reaction results and atom coordinates.

Data availability

X-ray data are available free of charge from the Cambridge Crystallographic Data Centre (https://www.ccdc.cam.ac.uk/data_request/cif) under reference numbers CCDC-1903723 (**1**), CCDC-1903724 (**2a**), CCDC-1903725 (**3**) and CCDC-1903726 (**4**). All other data generated or analysed during this study are included in the published article.

- Wilkerson, M. P., Burns, C. J., Paine, R. T. & Scott, B. L. Synthesis and crystal structure of $\text{UO}_2\text{Cl}_2(\text{THF})_2$: a simple preparation of an anhydrous uranyl reagent. *Inorg. Chem.* **38**, 4156–4158 (1999).
- Reynolds, J. G., Zalkin, A. & Templeton, D. H. Structure of uranyl nitrate-bis(tetrahydrofuran). *Inorg. Chem.* **16**, 3357–3359 (1977).
- Lalancette, J. M., Rollin, G. & Dumas, P. Metals intercalated in graphite. I. Reduction and oxidation. *Can. J. Chem.* **50**, 3058–3062 (1972).
- Liu, Y. et al. Mechanistic understanding of dinuclear cobalt(II) complex mediated highly enantioselective copolymerization of meso-epoxides with CO_2 . *Macromolecules* **47**, 7775–7788 (2014).
- Alexander, R. P. & Schroeder, H. Chemistry of decaborane–phosphorus compounds. IV. Monomeric, oligomeric, and cyclic phosphinocarboranes. *Inorg. Chem.* **2**, 1107–1110 (1963).
- Gaussian 09 (Gaussian Inc., 2010).
- Lee, C., Yang, W. & Parr, R. G. Development of the Colle–Salvetti correlation-energy formula into a functional of the electron density. *Phys. Rev. B* **37**, 785–789 (1988).
- Weigend, F. & Ahlrichs, R. Balanced basis sets of split valence, triple zeta valence and quadruple zeta valence quality for H to Rn: design and assessment of accuracy. *Phys. Chem. Chem. Phys.* **7**, 3297–3305 (2005).
- Cossi, M., Rega, N., Scalmani, G. & Barone, V. Energies, structures, and electronic properties of molecules in solution with the C-PCM solvation model. *J. Comput. Chem.* **24**, 669–681 (2003).
- Barone, V. & Cossi, M. Quantum calculation of molecular energies and energy gradients in solution by a conductor solvent model. *J. Phys. Chem. A* **102**, 1995–2001 (1998).
- Andzelm, J., Kölmel, C. & Klamt, A. Incorporation of solvent effects into density functional calculations of molecular energies and geometries. *J. Chem. Phys.* **103**, 9312–9320 (1995).

Acknowledgements We thank H. Zhou and G. Wu for assistance with NMR and XRD experiments, respectively. J. Kaare-Rasmussen is thanked for experimental support. The US-Israel Binational Science Foundation (grant 2016241), the ACS Petroleum Research Fund (58693-DNI3), the US Department of Energy, Office of Basic Energy Sciences (contract DE-SC-0001861), the University of California, Santa Barbara, and Tel Aviv University are thanked for financial support.

Author contributions M.K. carried out the synthetic work and analytical characterization, performed the electrochemical–chemical monophasic reactions and acquired most of the NMR and XRD data. C.H. devised the electrochemical setup and the mono- and biphasic experiments. T.G.C. and M.K. devised all the biphasic capture and release experiments. T.G.C. and V.K. synthesized precursor **1**. R.D. performed all DFT studies. M.K., C.H. and G.M. wrote the manuscript with input from all authors. R.D., T.W.H. and G.M. assisted with data analysis. G.M. directed the research.

Competing interests The authors declare no competing interests.

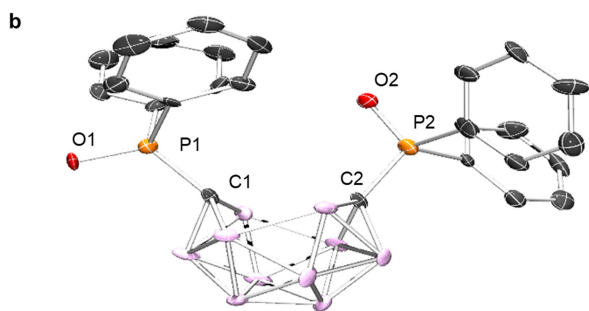
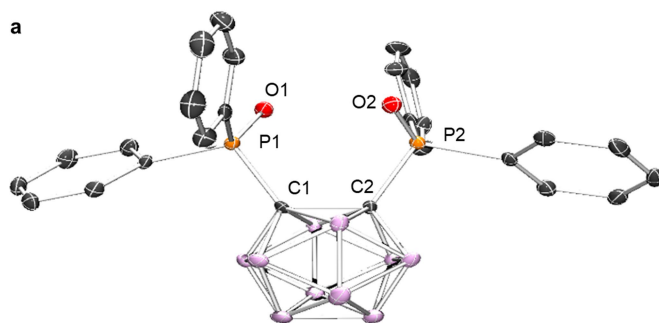
Additional information

Supplementary information is available for this paper at <https://doi.org/10.1038/s41586-019-1926-4>.

Correspondence and requests for materials should be addressed to G.M.

Peer review information Nature thanks Vincent Lavallo, Zuowei Xie and the other, anonymous, reviewer(s) for their contribution to the peer review of this work.

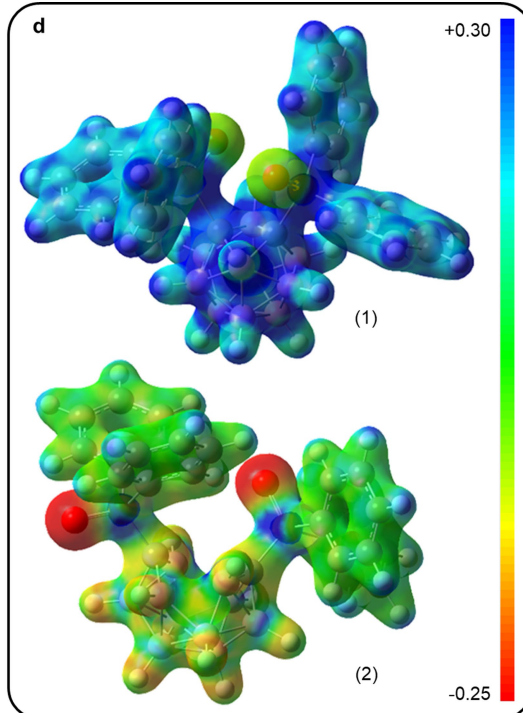
Reprints and permissions information is available at <http://www.nature.com/reprints>.



c

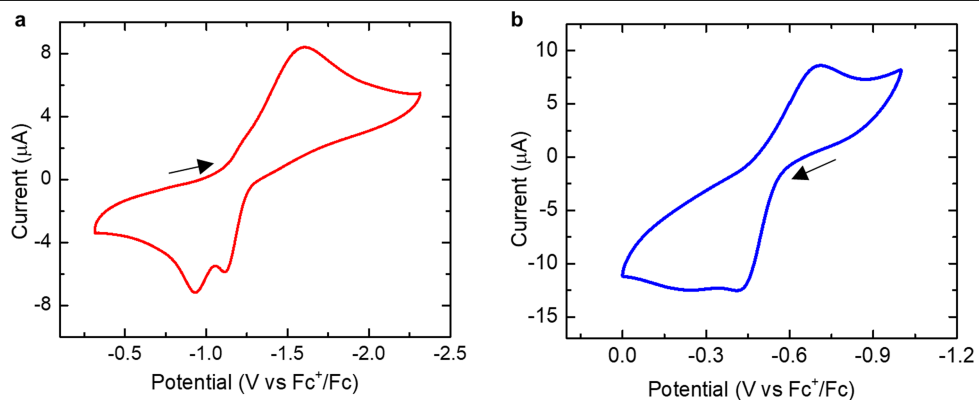
	1	2a	3*	4*
C···C	1.688(4) Å	2.860 Å	2.855 Å	2.857 Å
P···P	3.537 Å	5.036 Å	4.697 Å	4.806 Å
O1–U–O2			86.5(3)°	89.7(17)°

*Solid-state molecular structures 3 and 4 are shown in Figure 1.



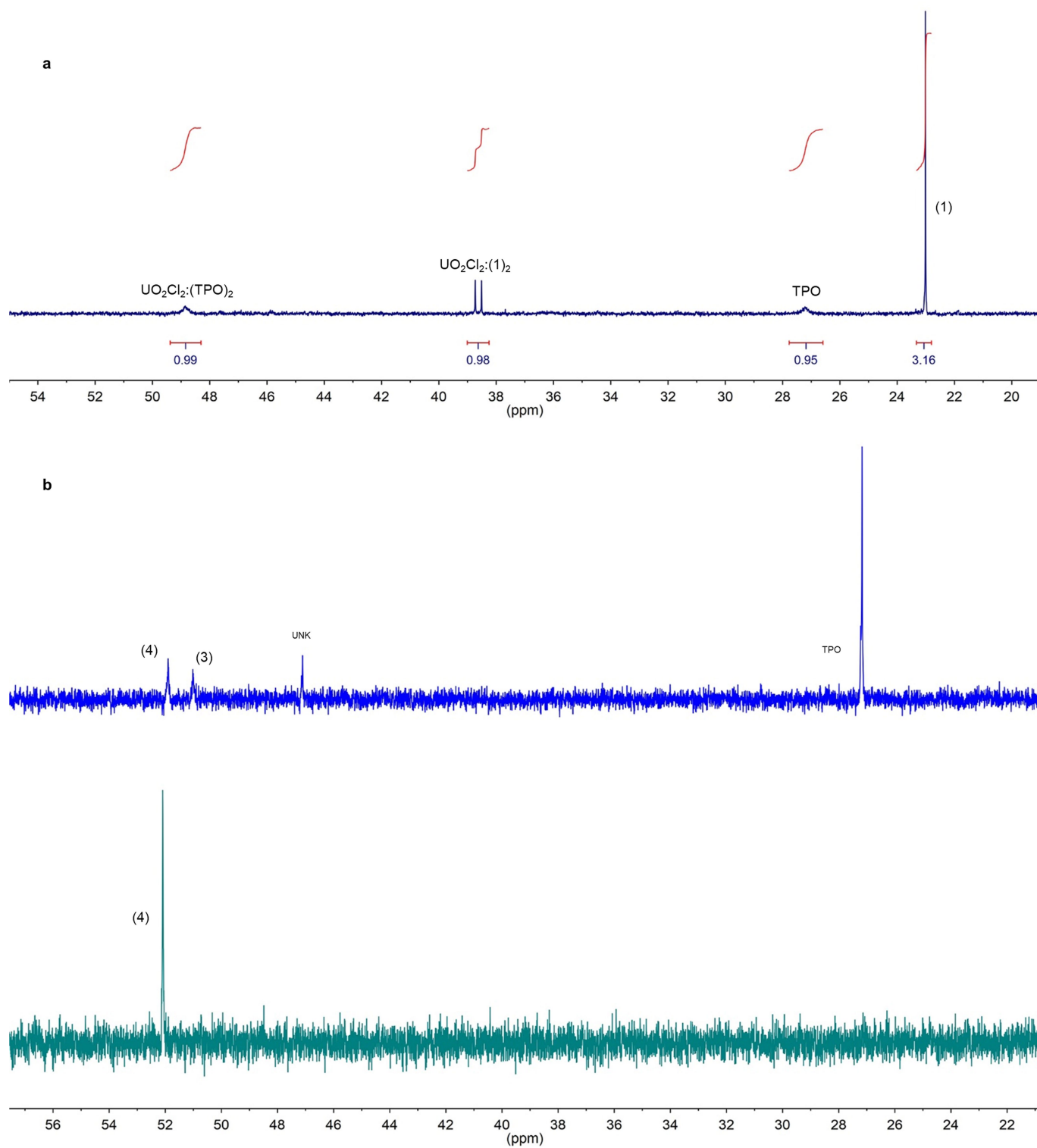
Extended Data Fig. 1 | Solid-state molecular structures and electron density surfaces. a, b, Solid-state molecular structures of complexes **1** (**a**) and **2a** (**b**). H atoms, $[\text{CoCp}_2]^+$ counter cations (**2a**) and all co-crystallized solvent molecules are omitted for clarity. **c,** Selected interatomic distances and angles

for complexes **1**, **2a**, **3** and **4**. **d,** Electron density surfaces with colour-coded electrostatic potentials obtained from DFT calculations using optimized structures of **1** and the anion of **2a**, labelled **2** (negative values (red) are indicative of higher electron density).



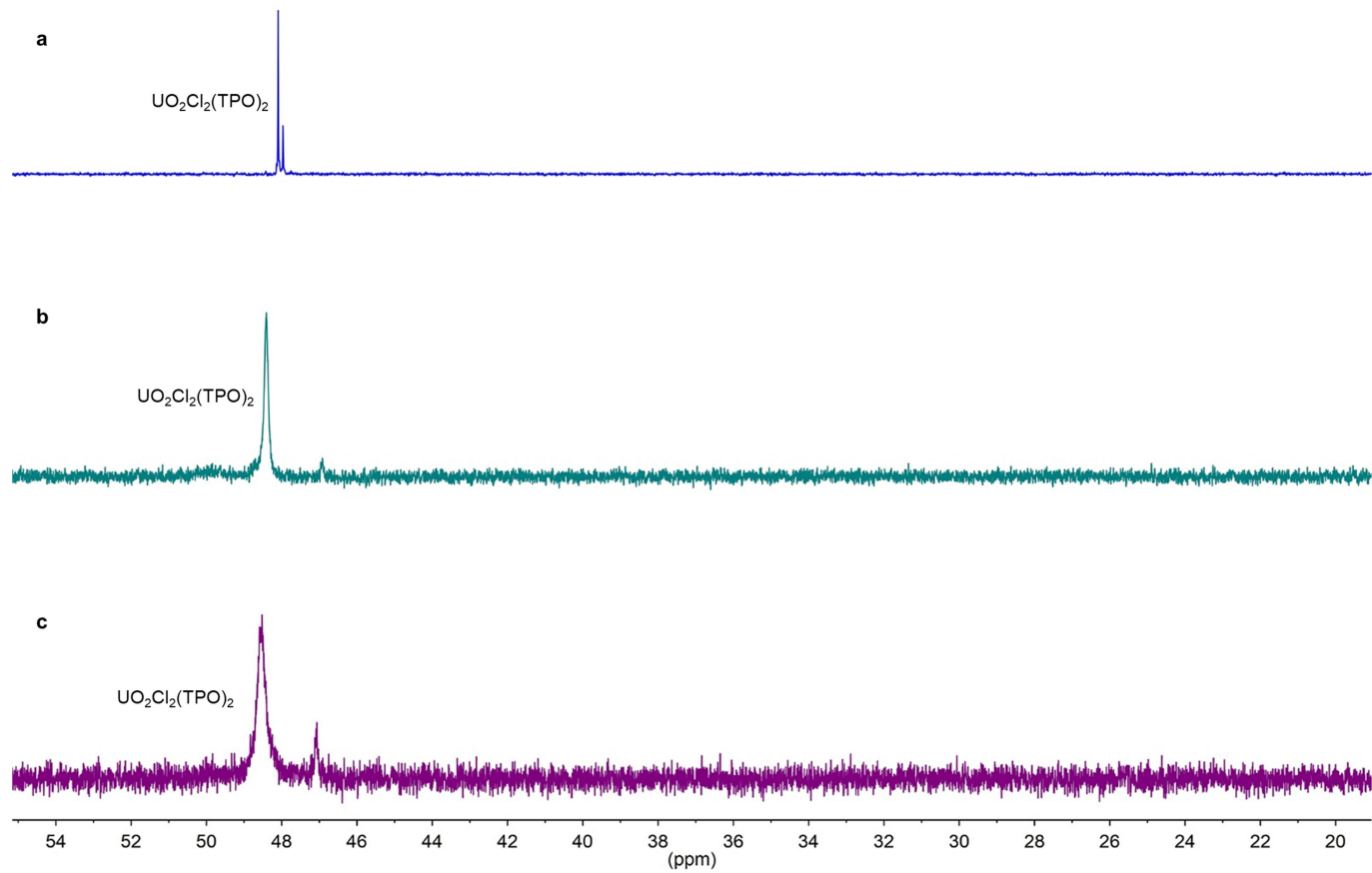
Extended Data Fig. 2 | Cyclic voltammetry data for 1 and 4. **a.** Cyclic voltammogram of **1** (0.5 mM) in a 0.1 M [Bu₄N][PF₆] THF solution, measured using a 3-mm-diameter glassy carbon working electrode and a platinum-wire counter electrode, referenced to the Fc^{+/0}/Fc redox couple (scan rate, 100 mV s⁻¹). The quasi-reversible redox event exhibits two cathodic waves at -0.93 V and

-1.11 V. **b.** Cyclic voltammogram of **4** (1.0 mM) in a 0.1 M [Bu₄N][PF₆] PC solution, obtained using a 3-mm-diameter glassy carbon working electrode and a platinum-wire counter electrode, referenced to the Fc^{+/0}/Fc couple (scan rate, 100 mV s⁻¹). The quasi-reversible redox event exhibits one anodic wave at -0.42 V.

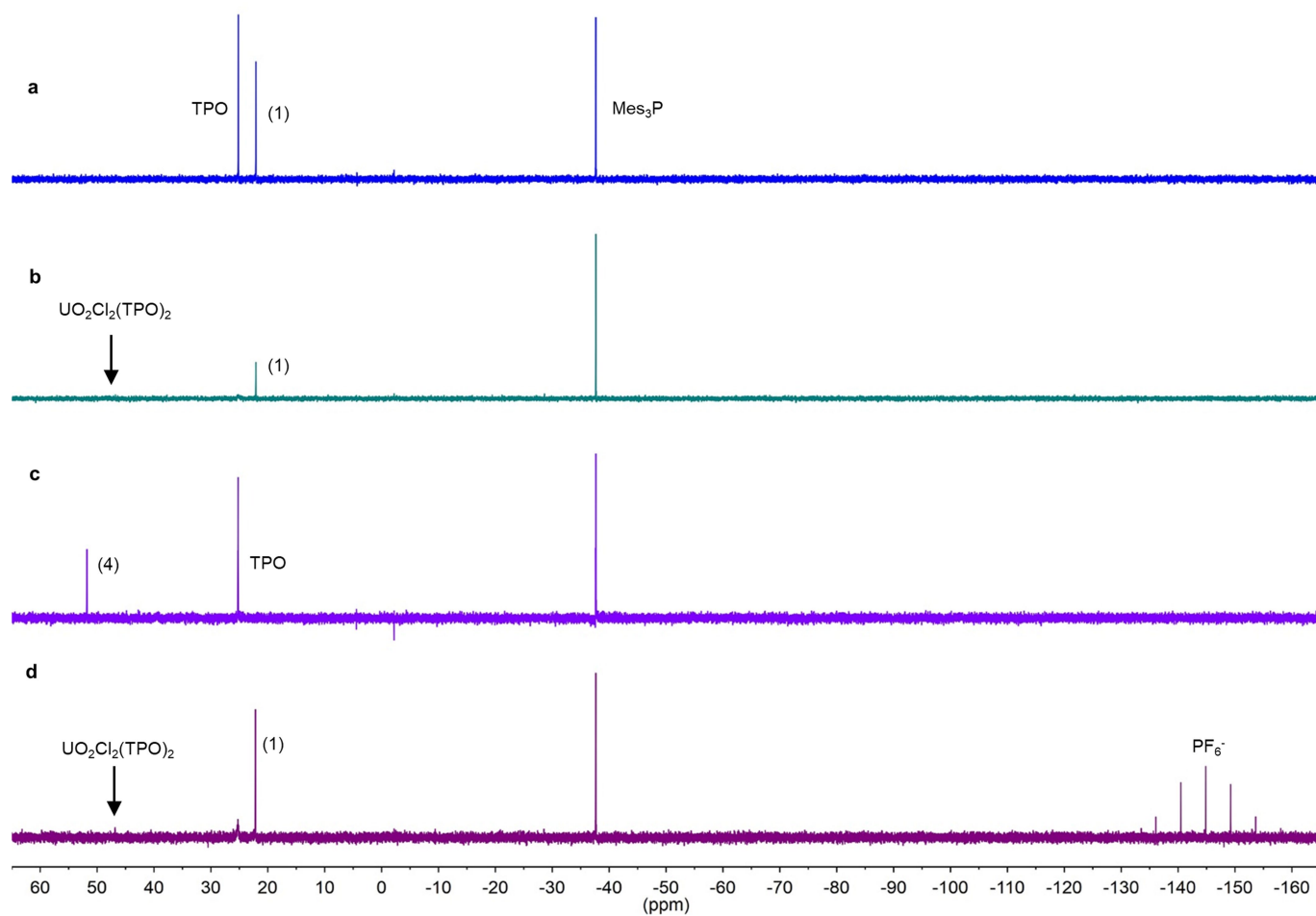


Extended Data Fig. 3 $^{31}\text{P}\{^1\text{H}\}$ NMR spectra from competition experiments of **1**, **2a** and TPO. **a**, $^{31}\text{P}\{^1\text{H}\}$ NMR spectrum of 2.0 equiv. **1** with 1.0 equiv. $\text{UO}_2\text{Cl}_2(\text{TPO})_2$ in DCM-d_2 . Relative integrations are shown in red. **b**, $^{31}\text{P}\{^1\text{H}\}$ NMR spectra of in situ reactions of 1.0 equiv. **2a** with 1.0 equiv. $\text{UO}_2\text{Cl}_2(\text{TPO})_2$ in

DCM-d_2 . Rapid precipitation of a yellow solid was observed. Top, $^{31}\text{P}\{^1\text{H}\}$ NMR spectrum of the DCM-d_2 supernatant. An unknown byproduct at 47 ppm is observed. Bottom, $^{31}\text{P}\{^1\text{H}\}$ NMR spectrum of the filtrate dissolved in PC with a DCM-d_2 capillary tube.

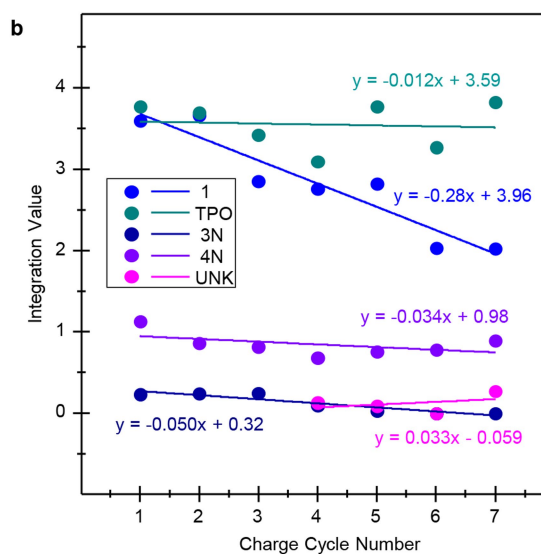
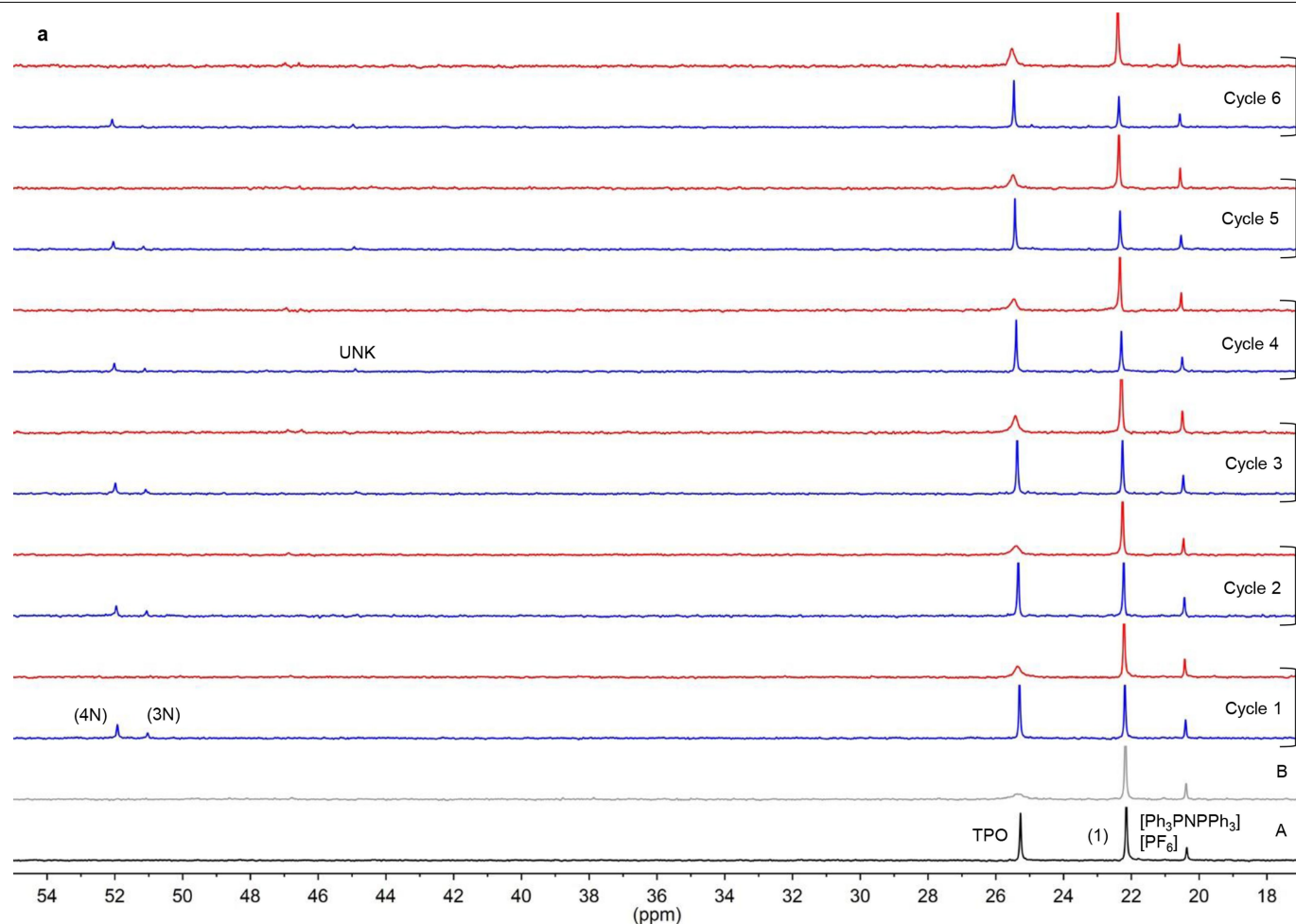


Extended Data Fig. 4 $^{31}\text{P}\{^1\text{H}\}$ NMR spectra from competition experiments of PC with $\text{UO}_2\text{Cl}_2(\text{TPO})_2$. **a.** Initial $^{31}\text{P}\{^1\text{H}\}$ NMR spectrum of $\text{UO}_2\text{Cl}_2(\text{TPO})_2$ in DCM-d_2 , displaying the proposed *cis:trans* isomers. **b.** $^{31}\text{P}\{^1\text{H}\}$ NMR spectrum after the addition of 20.0 equiv. PC to the solution in **a.** **c.** $^{31}\text{P}\{^1\text{H}\}$ NMR spectrum after the addition of 40.0 equiv. PC to the solution in **a.**



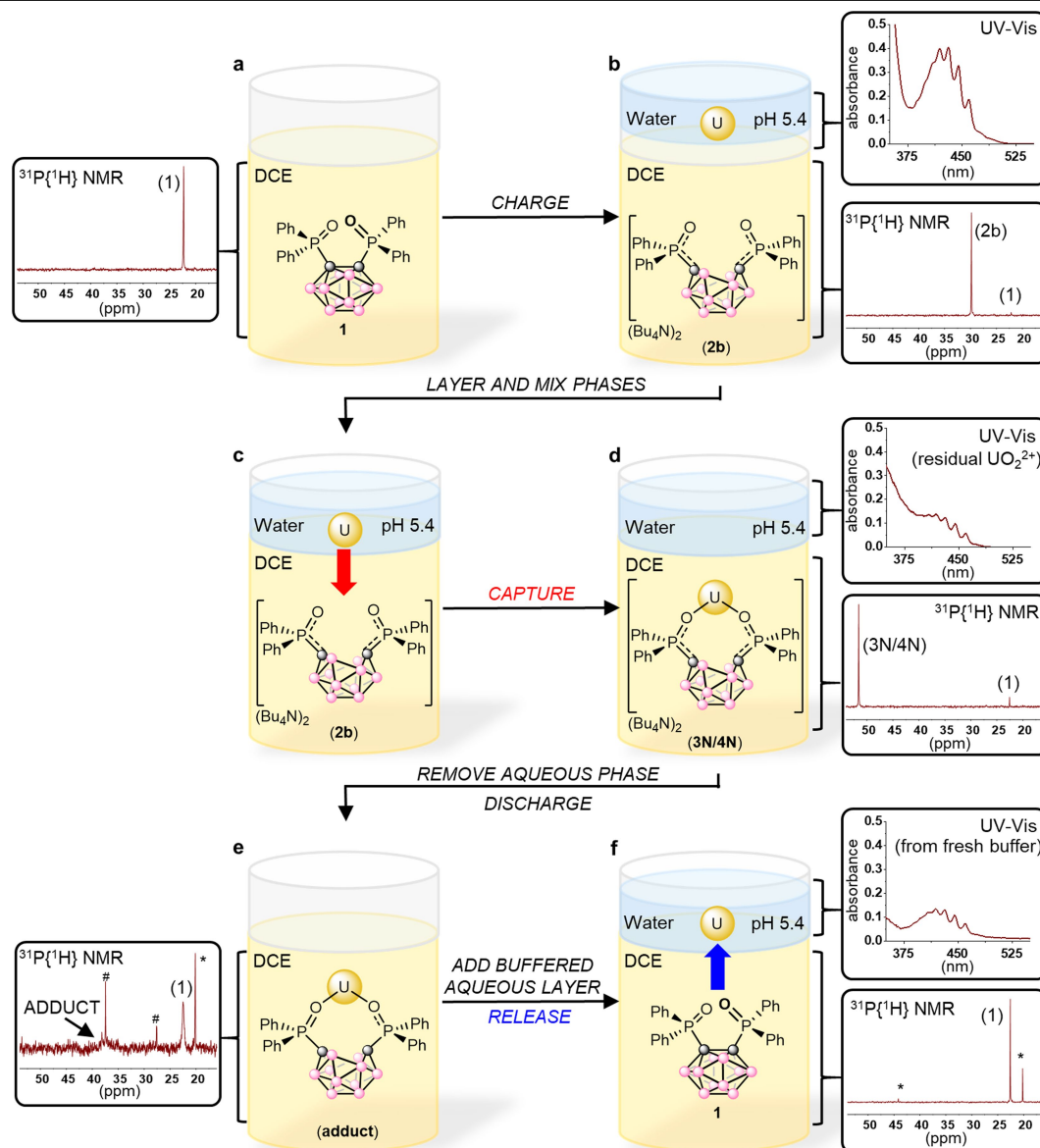
Extended Data Fig. 5 $^{31}\text{P}\{^1\text{H}\}$ NMR spectra for chemical capture and release of UO_2^{2+} . Reactions were carried out in a PC:benzene (3:1) solvent mixture with a MeCN-d_3 capillary tube insert using Mes_3P as the analytical standard. A relaxation delay of 30 s was used to obtain accurate integrations of all species (see Methods). **a**, $^{31}\text{P}\{^1\text{H}\}$ NMR spectrum of 4.0 equiv. TPO and 2.0 equiv. **1**.

b, $^{31}\text{P}\{^1\text{H}\}$ NMR spectrum of 4.0 equiv. TPO and 2.0 equiv. **1** in the presence of 0.5 equiv. $[\text{UO}_2\text{Cl}_2(\text{THF})_2]_2$. **c**, $^{31}\text{P}\{^1\text{H}\}$ NMR spectrum of 4.0 equiv. CoCp^*_2 added to the reaction in **b**. **d**, $^{31}\text{P}\{^1\text{H}\}$ NMR spectrum after addition of 4.0 equiv. $[\text{Fc}][\text{PF}_6]$ to the reaction in **c**. The reaction conditions are detailed in Methods.



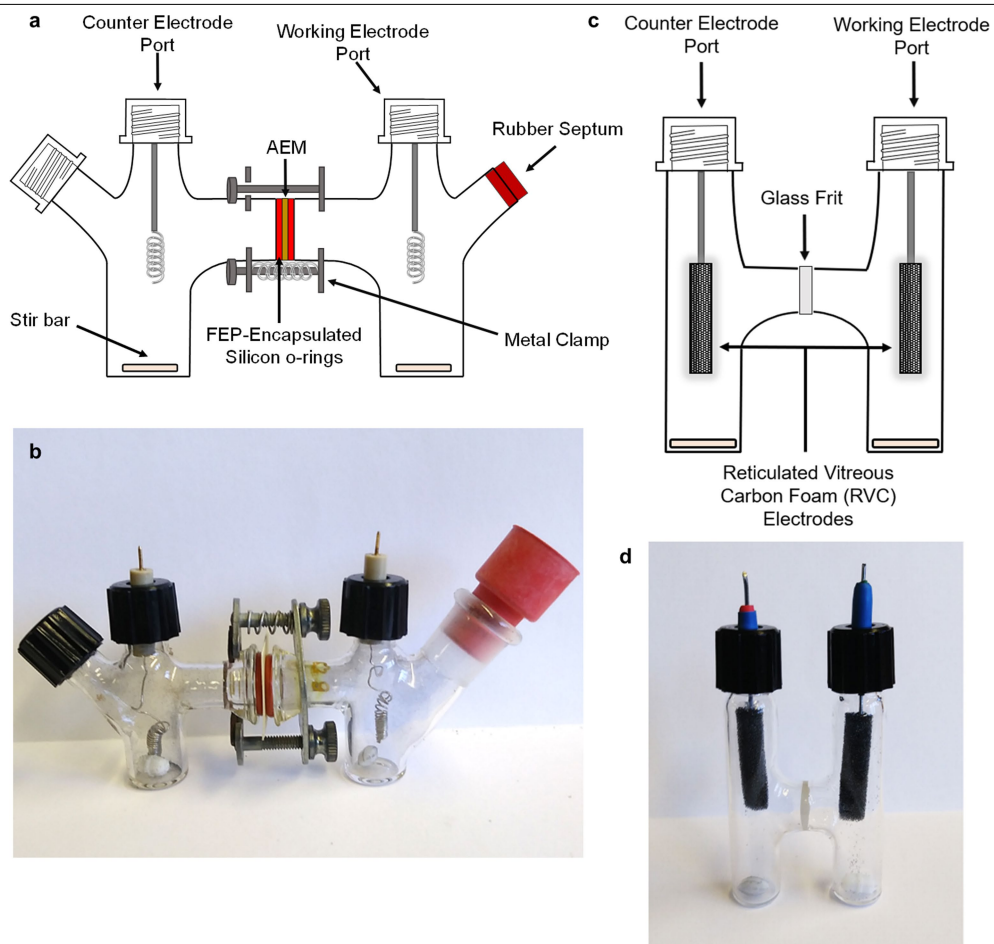
Extended Data Fig. 6 | Monophasic electrochemical capture and release of UO_2^{2+} by GBE. Reactions were carried out in a PC:benzene (3:1) solvent mixture with a MeCN-d_3 capillary tube insert with $[\text{Ph}_3\text{PNPPh}_3][\text{PF}_6]$ as the analytical standard. A relaxation delay of 40 s was used to obtain accurate integrations of all species (see Methods). **a**, A: $^{31}\text{P}\{^1\text{H}\}$ NMR spectrum of 6.0 equiv. TPO and 5.0 equiv. **1**, with 1.0 equiv. $[\text{Ph}_3\text{PNPPh}_3][\text{PF}_6]$ as the analytical standard. B: $^{31}\text{P}\{^1\text{H}\}$ NMR spectrum of 6.0 equiv. TPO and 5.0 equiv. **1** in the presence of 0.5 equiv. $[\text{UO}_2\text{Cl}_2(\text{THF})_2]$. Cycles 1–6: $^{31}\text{P}\{^1\text{H}\}$ NMR spectra of charged (blue) and discharged (red) solutions. An unknown species begins to appear at 45 ppm

after multiple cycles. Detailed experimental conditions are given in Methods. **b**, Plot of integrated values for all ^{31}P -containing species, obtained from the charged spectra versus the charge cycle number. The repeated cycling resulted in loss of electrochemically generated **3N** (average loss of 15.6% per cycle) due to presumed chloride migration over the anion-exchange membrane. There was little change in the yield of TPO (average loss of 0.3% per cycle) with larger losses in **1** (average loss of 7.2% per cycle) and **4N** (average loss of 3.4% per cycle). The values of per cent loss per cycle were estimated from the calculated trendlines by taking the ratio of the slope versus the y-intercept values.



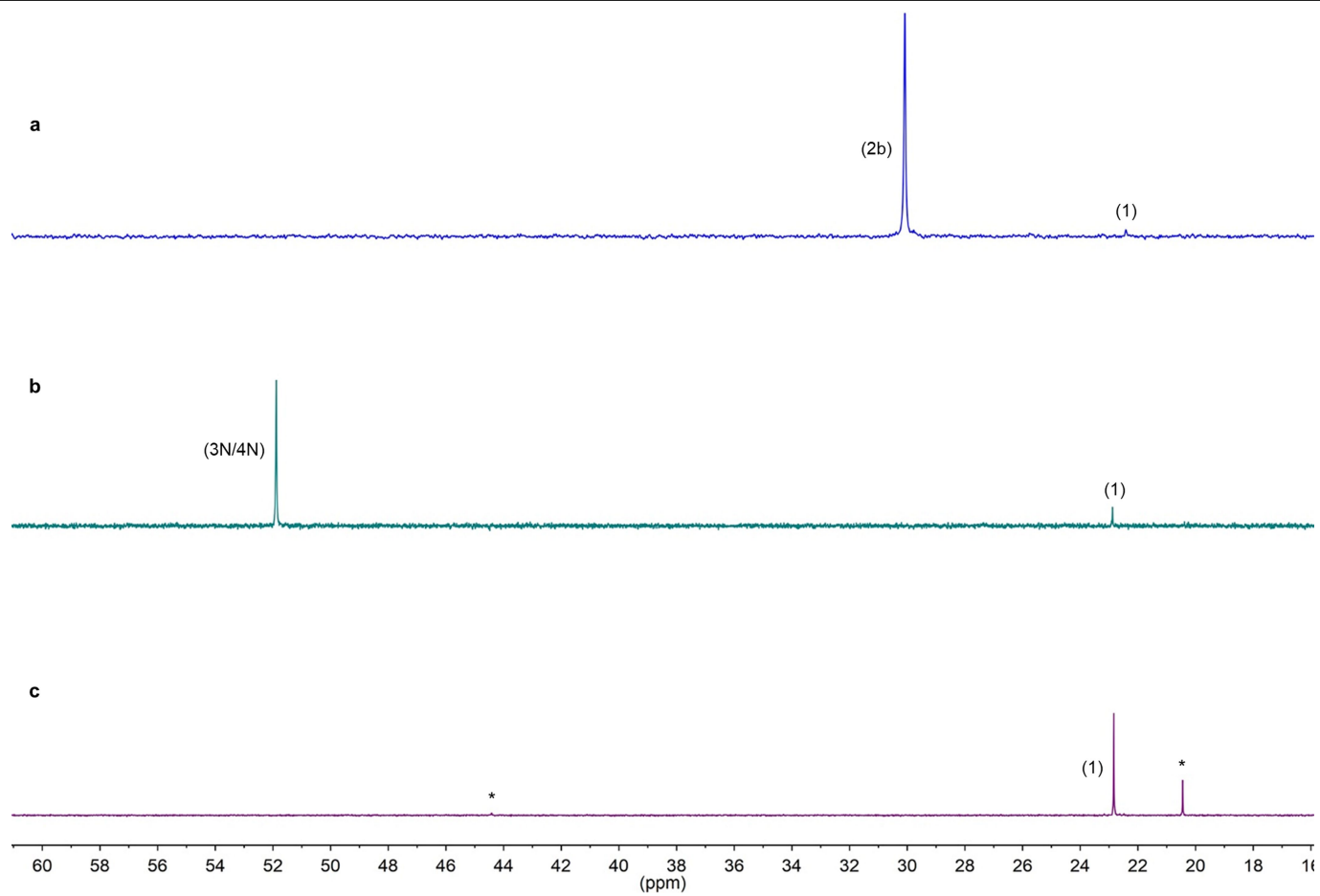
Extended Data Fig. 7 | Stepwise procedure for the biphasic electrochemical capture and release of UO_2^{2+} (yellow U). For simplicity, only half of the H-cell is displayed here. For the full cell design, see Extended Data Fig. 8c. **a**, $^{31}\text{P}\{^1\text{H}\}$ NMR spectrum of DCE layer containing only **1** and $[\text{Bu}_4\text{N}][\text{PF}_6]$ ($[\text{PF}_6]^-$ resonance not shown) before charging. **b**, Top inset, UV-Vis spectrum of aqueous phase containing 1.25 equiv. UO_2^{2+} (from $\text{UO}_2(\text{NO}_3)_2(\text{THF})_2$) before mixing with the DCE phase. Bottom inset, $^{31}\text{P}\{^1\text{H}\}$ NMR spectrum of DCE layer containing **2b** (major) and **1** (minor) after charging **1** (from **a**) galvanostatically. **c**, Mixing of the phases in **b** for 2 h. **d**, Top inset, UV-Vis spectrum of aqueous phase after mixing with the DCE phase, revealing approximately 0.35 equiv. UO_2^{2+} remaining. Bottom inset, $^{31}\text{P}\{^1\text{H}\}$ NMR spectrum of the DCE layer after mixing

with aqueous phase, showing captured products **3N/4N** (major) and **1** (minor). **e**, $^{31}\text{P}\{^1\text{H}\}$ NMR spectrum of the DCE layer following phase separation and galvanostatic discharge. A broad peak is observed at 38 ppm, which we attribute to an adduct of UO_2^{2+} with **1**. This, together with the broadened peak of **1**, accounts for ~75% of products. The remaining unknown byproducts are marked with # or *. **f**, Top inset, UV-Vis spectrum of aqueous phase after addition of fresh buffer to the discharged DCE solution (in **e**) and mixing for 12 h. The spectrum reveals the release of approximately 0.50 equiv. UO_2^{2+} . Bottom inset, $^{31}\text{P}\{^1\text{H}\}$ NMR spectrum of the DCE layer after mixing with fresh buffer, showing the free carborane **1** (major), as well as unknown byproducts at 44 ppm and 20 ppm marked by * (~20% of total).



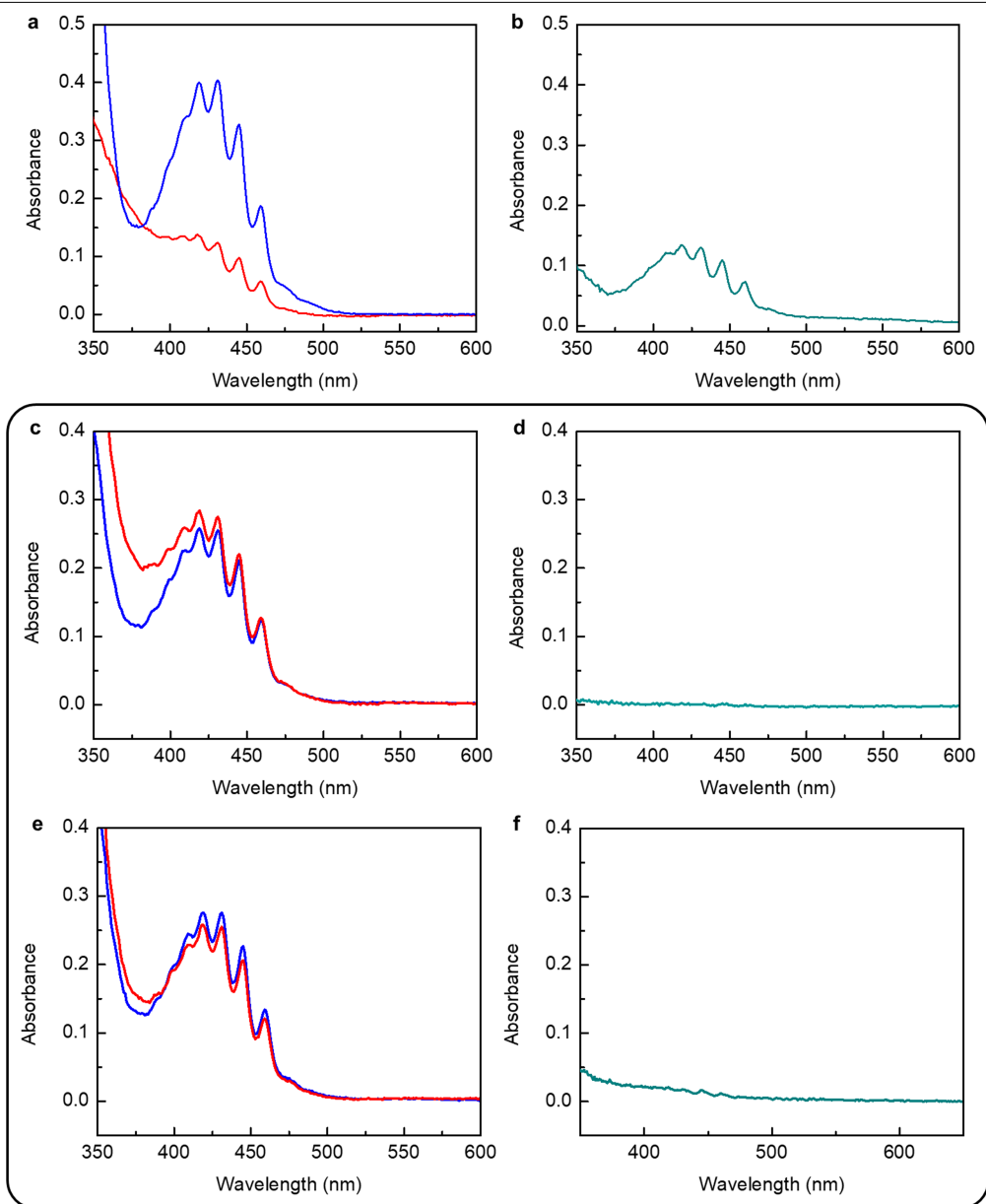
Extended Data Fig. 8 | Diagrams for mono- and biphasic electrochemical cells. **a**, Schematic of the divided H-cell used for the monophasic galvanostatic bulk electrolysis cycling experiments with UO_2^{2+} . **b**, Photograph of the divided H-cell used for the monophasic galvanostatic bulk electrolysis cycling

experiments with UO_2^{2+} . **c**, Schematic of the two-compartment H-cell used for the biphasic electrochemical capture and release of UO_2^{2+} . **d**, Photograph of the two-compartment H-cell used for the biphasic electrochemical capture and release of UO_2^{2+} .



Extended Data Fig. 9 | $^{31}\text{P}\{^1\text{H}\}$ NMR spectra for biphasic electrochemical capture and release of UO_2^{2+} . **a.** $^{31}\text{P}\{^1\text{H}\}$ NMR spectrum of electrochemically reduced **1** in DCE to produce **2b**. **b.** $^{31}\text{P}\{^1\text{H}\}$ NMR spectrum of DCE layer following UO_2^{2+} capture from the aqueous layer containing $\text{UO}_2(\text{NO}_3)_2(\text{THF})_2$ in 0.1M

sodium acetate buffer. **c.** $^{31}\text{P}\{^1\text{H}\}$ NMR spectrum of an electrochemically oxidized DCE layer containing **3N/4N** following extraction of UO_2^{2+} into 0.1M sodium acetate buffer. Minor unknown byproducts (marked by asterisks) are also observed. Detailed experimental conditions are found in Methods.



Extended Data Fig. 10 | UV-Vis spectra for the biphasic electrochemical capture and release of UO_2^{2+} and controls. **a**, Initial UV-Vis spectrum of $\text{UO}_2(\text{NO}_3)_2(\text{THF})_2$ (0.042 g, 0.078 mmol, 0.026 M, 1.25 equiv.) in 3 ml of 0.1 M sodium acetate buffer at pH 5.4 (blue). UV-Vis spectrum taken after mixing the aqueous layer with the DCE layer of electrochemically reduced **1** (to generate **2b**) in a 0.1 M $[\text{Bu}_4\text{N}][\text{PF}_6]$ DCE solution for 2 h, indicating a residual concentration of 0.0073 M, consistent with a total quantity of captured UO_2^{2+} to the DCE layer of 0.056 mmol (red). **b**, UV-Vis spectrum of 0.1 M aqueous sodium acetate buffer layer at pH 5.4 after mixing for 12 h with electrochemically oxidized **3N/4N** in DCE. The concentration of UO_2^{2+} was calculated to be 0.010 M, consistent with a total quantity of 0.031 mmol of released UO_2^{2+} from the DCE layer to the aqueous phase. **c**, Control for UO_2^{2+} migration from water to DCE in the absence of carborane (**1** or **2a/b**). Initial

UV-Vis spectrum of UO_2^{2+} in 0.1 M sodium acetate-buffered solution at pH 5.4 (blue). UV-Vis spectrum of aqueous layer after mixing for 4 h with DCE solution containing $[\text{Bu}_4\text{N}][\text{PF}_6]$ (0.1 M; red). **d**, Corresponding UV-Vis spectrum of DCE layer after mixing for 4 h with the aqueous layer containing UO_2^{2+} shown in **c**. **e**, Control for UO_2^{2+} migration from water to DCE in the presence of neutral carborane (**1**). Initial UV-Vis spectrum of UO_2^{2+} (1.0 equiv.) in 0.1 M sodium acetate-buffered solution at pH 5.4 (blue). UV-Vis spectrum of aqueous layer after mixing for 3 h with DCE solution containing $[\text{Bu}_4\text{N}][\text{PF}_6]$ (0.1 M) and **1** (1.0 equiv.; red). **f**, Corresponding UV-Vis spectrum of DCE layer containing **1** after mixing for 3 h with the aqueous layer containing UO_2^{2+} shown in **e**. The UO_2^{2+} extinction coefficient was experimentally determined to be $7.715 \text{ L mol}^{-1} \text{ cm}^{-1}$ (460 nm) at pH 5.4. See Methods for experimental details.